INSTITUTO POTOSINO DE INVESTIGACIÓN CIENTÍFICA Y TECNOLÓGICA, A.C.

POSGRADO EN CIENCIAS APLICADAS

Modeling and control of a three–level neutral point clamped converter by transient distortion of reference signal

Tesis que presenta

Lic. Víctor Manuel Rodríguez Zermeño

Para obtener el grado de

Maestro en Ciencias Aplicadas

En la opción de

Control y Sistemas Dinámicos

Director de la Tesis:

Dr. Gerardo Escobar Valderrama

San Luis Potosí, S.L.P., Septiembre de 2008

IPICYT

Constancia de aprobación de la tesis

La tesis "**Modeling and control of a three–level neutral point clamped converter by transient distortion of reference signal**" presentada para obtener el Grado de de **Maestro en Ciencias Aplicadas en la opción de Control y Sistemas Dinámicos** fue elaborada por **Víctor Manuel Rodríguez Zermeño** y aprobada el 19 de septiembre de 2008 por los suscritos, designados por el Colegio de Profesores de la División de Matemáticas Aplicadas del Instituto Potosino de Investigación Científica y Tecnológica, A.C.

Dr. Gerardo Escobar Valderrama
Director de la tesis

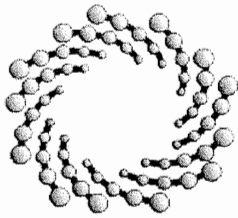Dr. Víctor Cárdenas Galindo
Sinodal

Dr. Arturo Zavala Río
Sinodal

Créditos Institucionales

Instituto Potosino de Investigación Científica y Tecnológica, A.C.

Acta de Examen de Grado

El Secretario Académico del Instituto Potosino de Investigación Científica y Tecnológica, A.C., certifica que en el Acta 017 del Libro Primero de Actas de Exámenes de Grado del Programa de Maestría en Ciencias Aplicadas en la opción de Control y Sistemas Dinámicos está asentado lo siguiente:

En la ciudad de San Luis Potosí a los 30 días del mes de septiembre del año 2008, se reunió a las 11:00 horas en las instalaciones del Instituto Potosino de Investigación Científica y Tecnológica, A.C., el Jurado integrado por:

Dr. Arturo Zavala Río	**Presidente**	**IPICYT**
Dr. Gerardo Escobar Valderrama	**Secretario**	**IPICYT**
Dr. Víctor Manuel Cárdenas Galindo	**Sinodal externo**	**UASLP**

a fin de efectuar el examen, que para obtener el Grado de:

MAESTRO EN CIENCIAS APLICADAS
EN LA OPCIÓN DE CONTROL Y SISTEMAS DINÁMICOS

sustentó el C.

Víctor Manuel Rodríguez Zermeño

sobre la Tesis intitulada:

Modeling and control of a three–level neutral point clamped converter by transient distortion of reference signal

que se desarrolló bajo la dirección de

Dr. Gerardo Escobar Valderrama

El Jurado, después de deliberar, determinó

APROBARLO

Dándose por terminado el acto a las 12:30 horas, procediendo a la firma del Acta los integrantes del Jurado. Dando fé el Secretario Académico del Instituto.

A petición del interesado y para los fines que al mismo convengan, se extiende el presente documento en la ciudad de San Luis Potosí, S.L.P., México, a los 30 días del mes de septiembre de 2008.

Dr. Marcial Bonilla Marín
Secretario Académico

L.C.C. Ivonne Lizette Cuevas Velez
Jefa del Departamento de Asuntos Escolares

INSTITUTO POTOSINO
DE INVESTIGACIÓN
CIENTÍFICA Y TECNOLÓGICA, A.C.

IPICYT
SECRETARIA ACADEMICA

A mis padres

Agradecimientos

Quiero agradecer primeramente a mi asesor, el Dr. Gerardo Escobar Valderrama por dirigir este trabajo de tesis. Y de manera muy especial reconocer su confianza, paciencia y apoyo. También quiero agradecer a mis compañeros del laboratorio de Procesamiento y Calidad de la Energía Eléctrica: Misael, Andrés, Michael y Raymundo por su amistad y constante ayuda.

A los Doctores Víctor Cárdenas Galindo y Arturo Zavala Río por aceptar ser mis sinodales y de manera especial por sus comentarios y correcciones enfocados a enriquecer este trabajo.

A mis maestros, en particular a la Dra. Elizabeth Huber y al Dr. David Lizárraga por haberme dado un verdadero ejemplo de profesionalismo y excelencia académica.

Al Dr. Raúl Balderas por su amistad y consejo.

A mi familia por todos estos años de apoyo incondicional.

Y muy especialmente a mi novia Analie por su apoyo, su cariño y por estar conmigo todos estos años en los que hemos crecido juntos.

Contents

Abbreviations

AC   Alternate Current

CHB   Cascade H – Bridge

DC   Direct Current

EMI   Electromagnetic interference

FFT   Fast Fourier Transform

HB-5   H-Bridge (5 levels)

IGBT   Insulate Gate Bipolar Transistor

NPC-3   Neutral Point Clamped (3 levels)

PI   Proportional – Integral

PWM   Pulse Width Modulation

THD   Total Harmonic Distortion

SVM   Space Vector Modulation

VSI   Voltage Source Inverter

Resumen

Modeling and control of a three–level neutral point clamped converter by transient distortion of reference signal

PALABRAS CLAVE: Calidad de la Energía, Corrección del factor de potencia, Convertidores de potencia multinivel, Conversión de potencia AC–DC, Electrónica de potencia, sistemas no lineales.

Utilizando la formulación de Euler–Lagrange, se desarrolla un modelo completo para el convertidor NPC–3 adecuado para efectos de diseño de control. Para introducir una entrada de control adicional, y utilizarla para alcanzar el objetivo de balanceo, una perturbación transitoria es añadida a la señal de referencia de corriente. Se propone un controlador y se estudia la estabilidad del sistema en el sentido de Lyapunov. Para probar el buen desempeño del controlador se llevaron a cabo simulaciones numéricas en las que se observaron resultados satisfactorios para el seguimiento y la regulación. Sin embargo, a partir de estas pruebas, se encontró un compromiso entre el balanceo y la distorsión armónica total, grosso modo, no es posible alcanzar el primero sin alterar al segundo.

Abstract

Modeling and control of a three–level neutral point clamped converter by transient distortion of reference signal

KEY WORDS: Energy quality, Power factor correction, Multilevel power converters, AC–DC Power Conversion, PWM power converters, Power electronics, Nonlinear systems.

Modeling via the Euler–Lagrange Formulation of the NPC–3 power converter is performed providing with a complete model suitable for control purposes. A transitory perturbation is added to the current reference signal to provide with an extra control input used to reach a balance objective. A controller is proposed and its stability in the sense of Lyapunov studied. To test the performance of the controller, numerical simulations are performed, obtaining satisfactory overall results for tracking and regulation. Nevertheless, a tradeoff between balance and the THD reduction of the inductor's currents prevents from reaching full balance.

Introduction

1.1 Motivation

Recent analysis about the global trends in electric power consumption, reveal an important rise of the power needs in the forthcoming years [1]. In particular, within general electronics, power electronics has become in the last years one of the most active and evolved fields. This originated, mainly by the reduction in the production costs and a more affordable price of most electronic devices, this drives to the rise in the use of electronic equipment. However, this rise in the number of electronic devices plugged into the power grid promotes a decrement in the power quality of the supplied energy due to harmonic contamination injection by the electronic equipment [2]. Several requirements in current international standards, such as IEEE-519, IEC-61000, IESNA-PQ-4, ABS-150 and CFE-L00045 among others have been established. Therefore, a very active field of study is the one dedicated to achieve a minimum harmonic injection by electronic equipment to the grid [3]-[7].

Moreover, massive use of fossil combustibles leads to problems in the near future, such as, environmental contamination, resources limitation and subsequent cost increments. Consequently, the use of renewable energies and their efficient connection to the electric grid is a vast field of work, and very active these days. In addition, along with the technical evolution, a rising demand for converters rated at higher power, more and more efficient, also takes place.

As a consequence of the aforementioned issues, new and improved solutions within power electronics have been developed such as: new semiconductor devices (IGBTs and diodes) with high cosmic radiation withstand capability, new control and commutation strategies and new topologies such as multilevel converters. Due to their design, multilevel power converters portray suitable attributes to meet both power and quality requirements, especially in high power and renewable power sources applications.

Multilevel power converters have consolidated in the last years as a very important option in electric energy processing in the medium–high power range, from the technical point of view to the economic one; given that a significant increment can be evidenced in the applications where energy conversion is performed using multilevel power converters. The term, "multilevel" is applied to an inverter of three or more levels and was initially introduced by Nabae et all in 1981 [7]. Ever since, power electronics community and industry have driven all efforts in research and development of these converters. Being a technology of continuous growth, multilevel power converters have been used for a wide range of applications [8]:

- Power generation.
- Power transmission and distribution.
- Multiple industrial applications: rolling mills, fans, pumps and conveyors, marine appliances, mining and traction.
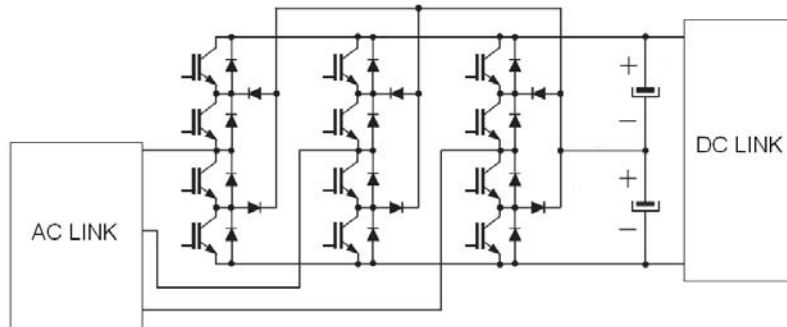- Active filtering for harmonic mitigation [9], [10].

Figure 1.1 The three level NPC–3 topology.

1.2 Background

Along with all aforesaid applications, the need for AC–DC conversion with low harmonic distortion and EMI has also relied in the multilevel converters [11]. It is desired for a AC–DC converter plugged into the grid to work with the highest possible power factor (closest to 1) in the AC link while a regulated output is needed in the DC link. During the last years, low and medium switching frequency devices, made the NPC–3 presented in Figure 1.1 a competitive and widely spread topology for a large variety of applications [12] including AC–DC conversion. Currently, high switching frequency devices such as the IGBT make it highly attractive for applications with a high number of operation hours per year, and specifically in countries with high energy costs [13]. A recent comparative study [12] outlines some of the longstanding advantages of the NPC–3 power converter such as a moderate expense in the input filter and the possible modular realization of common dc bus configuration, therefore, making it very competitive for a large variety of low and medium switching frequency applications despite the required high installed switch power. Although works, such as the one described in [23], present a mathematical model suitable for control purposes for the aforementioned NPC–3 topology, the lack of isomorphisms for control input transformations forces to a required balance for the capacitors voltages, in such a way that the model remains valid. Following all the previous arguments, it is evident the convenience

3

of having a complete and accurate mathematical model for the NPC–3 converter used as a synchronous rectifier.

A recent work [19] shows a strategy for controlling the HB–5 converter by introducing transitory extra control inputs. It is believed that approaches based on similar ideas could lead to controllers for other multilevel converter topologies, where the number of levels make necessary the introduction of extra control inputs. Therefore, a constructive method for addition of extra control inputs by means of introducing transitory terms in the current reference will be investigated for the case of the NPC–3 converter.

1.3 Contributions

The present work shows the following main contributions:

1. A model for the NPC–3 converter in a synchronous rectifier application is investigated. Emphasis is made upon the fact that only isomorphic relations are used for both coordinate and control input transformations. Therefore a complete model suitable for control purposes is generated. Also, use of a piecewise linear representation of the switching stage in the Euler–Lagrange Formulation leads to an uncomplicated model representation.

2. Encouraged by a recent work [19], where extra degrees of freedom are introduced as perturbations, a constructive method to introduce extra control inputs by transient perturbation of the current reference signal is formulated. In this work, one of the introduced control inputs will be used to solve the balance objective.

1.4 Thesis outline

In chapter 1 the motivation, background and main contributions of this work are presented. In chapter 2, the NPC–3 topology in a synchronous rectifier application is studied and modeled via the Euler–Lagrange formulation and control objectives are introduced. In chapter 3, a controller based on the previously proposed model is designed. Also Stability analysis is performed. Chapter 4 shows the results for numerical simulations. A steady state error prevents the capacitors voltages from achieving complete balance. Further investigation shows a tradeoff between the inductors' currents THD and the balancing objective. Some concluding remarks and a brief scope of the future work is given Chapter 5.

Problem formulation: Euler–Lagrange modeling and control objectives

2.0 Introduction

In this chapter, the NPC–3 topology in a synchronous rectifier application is studied and modeled via the Euler–Lagrange formulation. For the conversion stage, the array of Insulated–Gate Bipolar Transistors (IGBTs) in combination with diodes are considered as being ideal switches. To work with a continuous control signal, a multicarrier phase–shifted modulation algorithm at a relatively high switching frequency is employed to reduce the harmonic content of the switched signal. Coordinate transformations are applied when necessary to express the natural states of the system with more clarity and to simplify the controller design. To take advantage of the fact that no fourth wire is considered, and assuming that the source voltages do not exhibit homopolar component, a $123 \rightarrow \alpha\beta\gamma$ linear transformation is used. Finally, control objectives are introduced at the end of this chapter.

2.1 The NPC–3 converter

In the NPC–3 converter topology, under study here, three stages can be easily indentified: The AC or power input stage, the switching or conversion stage and the DC or power output stage. For this particular application, the converter is used as a synchronous rectifier; however other applications including active filtering or back–to–back AC to AC power conversion can be derived from this scheme quite easily.

Here, ideal switches allow the current from each source (i_1, i_2 or i_3) to take any desired path (i_{dc1}, i_{dc2} or i_{dc3}) when driven by the proper modulation scheme and duty cycle. The classical NPC–3 converter is shown in Figure 2.1 where:

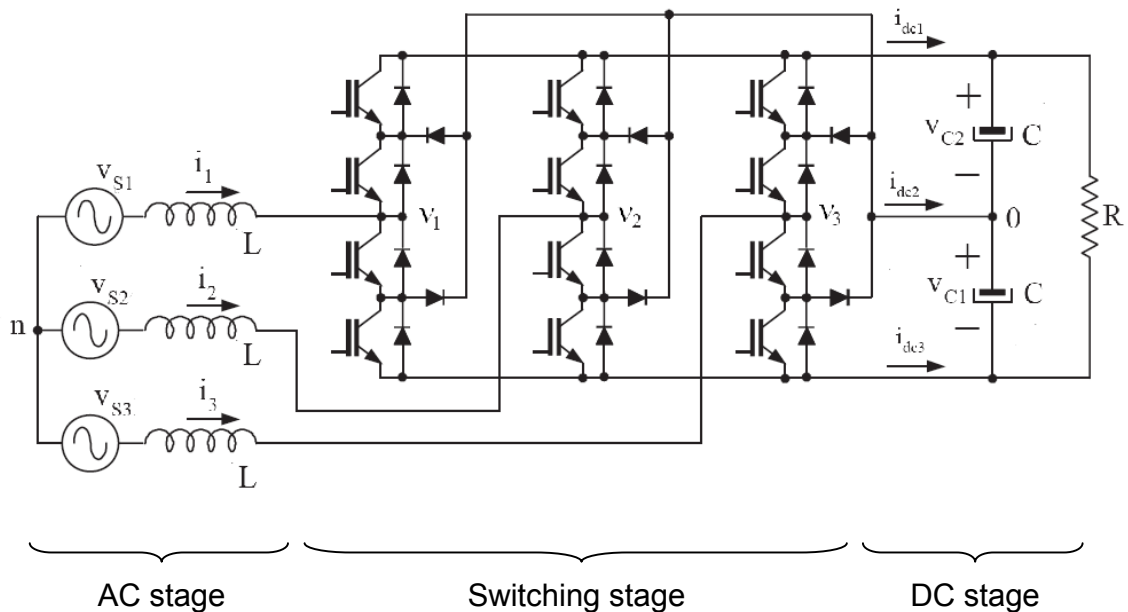|	
v_{S1}, v_{S2}, v_{S3}	: source voltages referred to "n"
i_1, i_2, i_3	: inductors currents
v_1, v_2, v_3	: voltages referred to "0"
v_{0n}	: voltage at "0" referred to "n"
L	: inductance of input inductors
C	: capacitance of output capacitors
R	: load resistance
i_{dc1}, i_{dc2}, i_{dc3}	: currents at top, middle and bottom connection points of capacitors
i_{C1}, i_{C2}	: capacitors currents

Figure 2.1 The three level NPC–3 inverter used as a synchronous rectifier. The AC stage includes the power sources and inductors. The switching stage is composed by the IGBTs and diodes assembly. Finally, capacitors and resistors conform the DC stage. The "neutral point" is denoted by "0", which is different of point "n".

2.2 Switching stage modeling

The IGBT works as an intermittent controlled diode. It allows electric current to flow in a single direction when the input signal is set to ON and prevents any flow to pass in any direction when its status is set to OFF. When connected in parallel with a diode, this construction can work as a controlled switch.

To easily model the NPC–3 converter, the IGBT– diode assemblies are assumed to be equivalent to ideal switches as shown in Figure 2.2. For simplicity and without loss of generality, a numerical value is assigned for each different position of the switches: "1" when it is connected to the top of the second capacitor; "0" when it is connected to the middle point between the capacitors and "–1" when it is connected below the first capacitor.
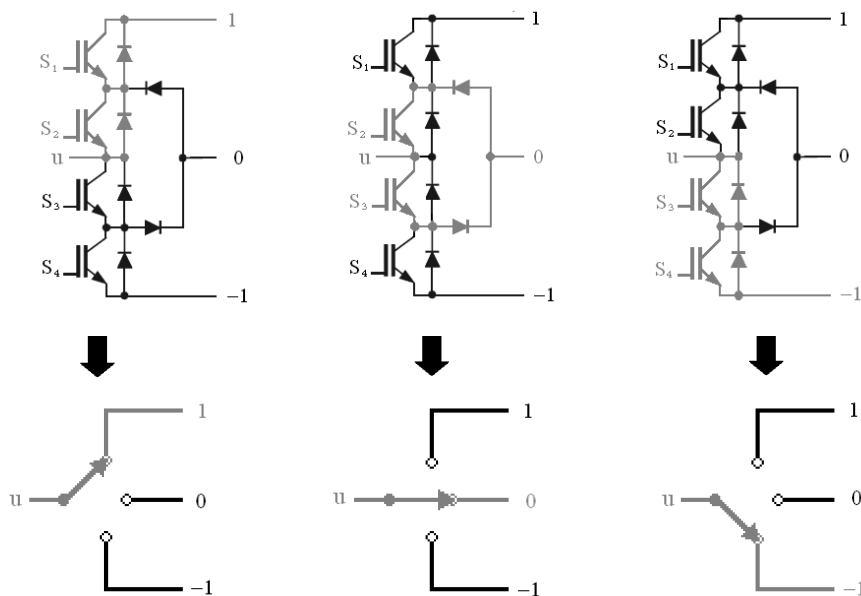

Figure 2.2 Simplification of switching stage for one of the phases. Each configuration of the IGBT states (S_1, S_2, S_3 and S_4) is simplified as the position of an ideal switch (u) with multiple positions.

The relation among the switch positions and the IGBT states can be directly determined from the circuit in Figure 2.2 as shown in Table 2.1. Notice the complementary IGBT pairs S1–S3 and S2–S4. The symmetry present in this converter will contribute in the model simplification and controller design as it will be seen in the next section.

Switch position (u)	IGBT state			
	S_1	S_2	S_3	S_4
1	On	On	Off	Off
0	Off	On	On	Off
−1	Off	Off	On	On

Table 2.1 Relation among the switch position (u) and the IGBT status.

Figure 2.3 shows a simplified version of the overall circuit where ideal switches are assumed. The voltages v_1, v_2 and v_3 are referred to the "0" node.
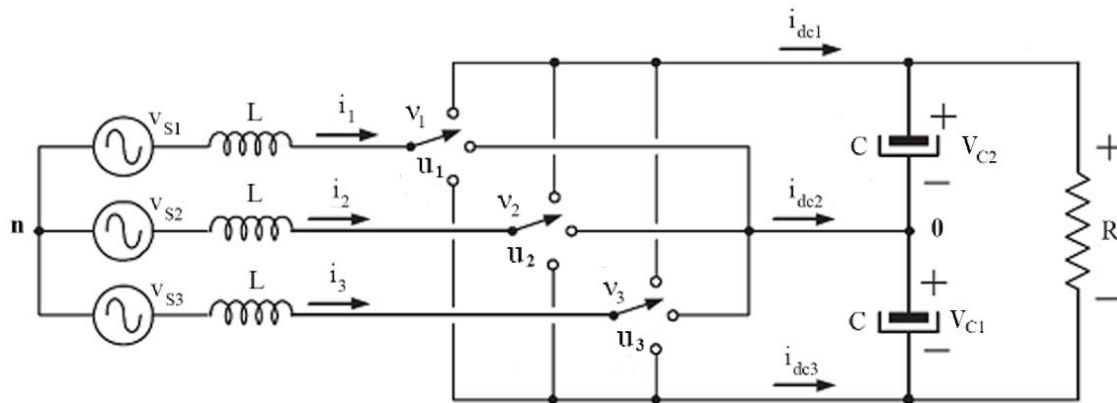

Figure 2.3 Simplified version of the circuit shown in Figure 2.1. Here, the IGBT–diode assemblies are considered as being ideal switches.

It is important to notice that, although Table 2.1 suggests a direct map among the switch positions u_k (k=1,2,3) and the IGBT's states, such relation would not be

practical since the former u_k would be restricted to take values in the discrete set *{1,0, −1}*. In order to consider a continuous range for the control signal u_k to the closed interval [−1,1] a multicarrier phase–shifted modulation algorithm is employed at a relatively high switching frequency [14]. This modulation scheme is intended to reduce the harmonic content of the switched signal while mapping the control switching positions to the IGBTs.

2.3 Euler–Lagrange Formulation

Modeling of the NPC–3 converter topology is based on the following assumptions:
- Voltage sources are assumed to be balanced, periodic sinusoidal signals of a known fundamental frequency.
- Capacitors and inductances are assumed to be ideal, no parasitic resistive elements are considered.
- The load is assumed to be linear.

Following [15], a generalized coordinate q_k and its time derivative are assigned to each of the energy storage elements:

$$q_k, \dot{q}_k : \ k \in \left\{ L_1, L_2, L_3, C_1, C_2 \right\}$$

where each generalized coordinate refers to a *generalized charge*. For the capacitors, the actual charge is used; while for the inductors, it is the time integral of the current passing through, i.e., the electric flux. The latter can be seen as a simple auxiliary variable. In a similar way, the time derivative of the generalized coordinates refers to *generalized currents*. For the inductors, the actual current is used, while for the capacitors, it is used the time derivative of the stored charge. Again, this latter definition is just for auxiliary purposes. Therefore the following coordinate transformation can be established:

$$
\begin{bmatrix}
\dot{q}_{L_1} \\
\dot{q}_{L_2} \\
\dot{q}_{L_3} \\
q_{C_1} \\
q_{C_2}
\end{bmatrix}
=
\begin{bmatrix}
i_1 \\
i_2 \\
i_3 \\
CVc_1 \\
CVc_2
\end{bmatrix}
$$

It is important to notice that the Current Kirchhoff's Law imposes a semi–holonomic constraint to the Euler–Lagrange formulation [16]. For this reason, and to properly express the dynamics, a secondary equation, including the aforementioned constraints, is used as described in [15]. Hence, with the previously defined *generalized charges* and *currents*, the complete Euler–Lagrange formulation for the NPC–3 is expressed as follows:

$$
\frac{d}{dt}\left(\frac{\partial \mathfrak{L}}{\partial \dot{q}}\right) - \left(\frac{\partial \mathfrak{L}}{\partial q}\right) = -\left(\frac{\partial \mathfrak{D}_u}{\partial \dot{q}}\right) + A\lambda + \mathfrak{F} \tag{2.1}
$$

$$
A^T \dot{q} = 0 \tag{2.2}
$$

where:

$\mathfrak{L}$:   Lagrangian of the system

q :   Generalized coordinates vector

$\mathfrak{D}_u$:   Rayleigh dissipation function

A :   Restrictions matrix

λ :   Lagrange multipliers vector

$\mathfrak{F}$:   Generalized force

Observe that, a feature of the Euler–Lagrange formulation is that the voltages v_{0n}, v_1, v_2 and v_3 do not need to be explicitly handled as in the case of direct application of Kirchhoff's laws. Instead, only generalized coordinates and control inputs along with the Lagrange multipliers are required to provide with a complete model. Thus, no particular assumption is made about the nature of the aforementioned voltages. In particular, the Euler-Lagrange approach does not

imply at any moment that voltage v_{0n} is zero. Considering the kinetic energy as a function of the inductor's currents, and the potential energy as a function of the charge in the capacitors, then the Lagrangian can be expressed as:

$$\mathfrak{L} = \frac{1}{2} L \left(\dot{q}_{L_1}^{\;2} + \dot{q}_{L_2}^{\;2} + \dot{q}_{L_3}^{\;2} \right) - \frac{1}{2C} \left(q_{C_1}^{\;2} + q_{C_2}^{\;2} \right) \tag{2.3}$$

The Rayleigh's dissipation function includes all energy losing components. In this case the load resistor only. Using the unit step function $\theta(\cdot)$, this is expressed as:

$$\mathfrak{D}_u = \frac{1}{2} R \left(\sum_{j=1}^{3} \theta(u_j) u_j \dot{q}_{L_j} - \dot{q}_{C_2} \right)^2 \tag{2.4}$$

where:

$$\left(\sum_{j=1}^{3} \theta(u_j) u_j \dot{q}_{L_j} - \dot{q}_{C_2} \right) = \left(\sum_{j=1}^{3} \theta(-u_j) u_j \dot{q}_{L_j} - \dot{q}_{C_1} \right)$$

is the current passing through the resistor.

Figure 2.4 shows the NPC–3 topology with the state variables expressed as *generalized charges* and *currents.* The arrows point out the nodes where the semi–holonomic constraints are established. The intermittent nodes at the switching stage will be assumed either closed or opened as a function of input u_k *(k=1,2,3).* Therefore, constraint equations can be stated as follows:

$$\sum_{j=1}^{3} \dot{q}_{L_j} = 0 \tag{2.5}$$

$$\sum_{j=1}^{3} \theta(u_j) u_j \dot{q}_{L_j} - \dot{q}_{C_2} = \frac{q_{C_1} + q_{C_2}}{R\,C} \tag{2.6}$$

$$\sum_{j=1}^{3} \left(1 - |u_j| \right) \dot{q}_{L_j} - \dot{q}_{C_1} + \dot{q}_{C_2} = 0 \tag{2.7}$$

$$-\sum_{j=1}^{3} \theta\left(-u_{j}\right) u_{j} \dot{q}_{L_{j}} + \dot{q}_{C_{1}} = -\frac{q_{C_{1}} + q_{C_{2}}}{R\, C} \qquad (2.8)$$
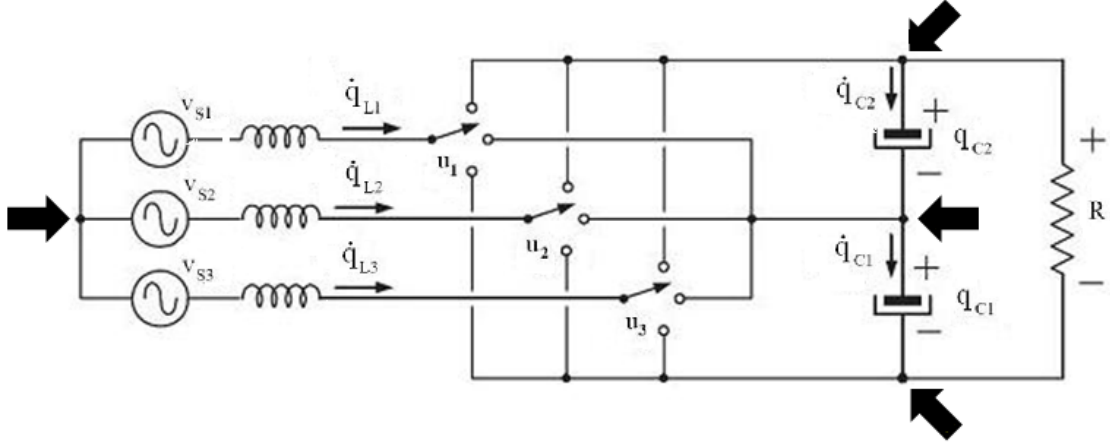
Figure 2.4 NPC–3 inverter using *generalized charges* and *currents*. The thick arrows indicate the nodes where the semi–holonomic constraints are established.

Using Ohm's law, it can be easily noticed that equations (2.6) and (2.8) were already considered while constructing the Rayleigh dissipation function. So, only equations (2.5) and (2.7) will be taken into account in the constraints matrix. Also observe that subtracting equation (2.5) from equation (2.7) leads to a simpler expression:

$$\sum_{j=1}^{3} \left| u_{j} \right| \dot{q}_{L_{j}} + \dot{q}_{C_{1}} - \dot{q}_{C_{2}} = 0 \qquad (2.9)$$

Hence, the constraints matrix can be written as:

$$A = \begin{bmatrix} 1 & \left| u_{1} \right| \\ 1 & \left| u_{2} \right| \\ 1 & \left| u_{3} \right| \\ 0 & 1 \\ 0 & -1 \end{bmatrix} \qquad (2.10)$$

Based on the later simplification, the Lagrange multiplier vector will be:

$$\lambda = \begin{bmatrix} \lambda_1 \\ \lambda_2 \end{bmatrix} \tag{2.11}$$

Finally, the generalized forces term is:

$$\mathfrak{F} = \begin{pmatrix} v_{s1} & v_{s2} & v_{s3} & 0 & 0 \end{pmatrix}^T \tag{2.12}$$

Here, voltages v_{S_1}, v_{S_2} and v_{S_3} are assumed to be periodic sinusoidal signals of a known fundamental frequency denoted by ω fulfilling the condition:

$$v_{S_1} + v_{S_2} + v_{S_3} = 0$$

Substituting equations (2.3), (2.4), (2.10), (2.11) and (2.12) in equations (2.1) and (2.2), the Euler–Lagrange formulation of the system is presented as follows:

$$L\begin{pmatrix} \ddot{q}_{L_1} \\ \ddot{q}_{L_2} \\ \ddot{q}_{L_3} \\ 0 \\ 0 \end{pmatrix} + \frac{1}{C}\begin{pmatrix} 0 \\ 0 \\ 0 \\ q_{C_1} \\ q_{C_2} \end{pmatrix} = -R\left(\sum_{j=1}^{3} \dot{q}_{L_j}\theta(u_j)u_j - \dot{q}_{C_2}\right)\begin{pmatrix} \theta(u_1)u_1 \\ \theta(u_2)u_2 \\ \theta(u_3)u_3 \\ 0 \\ -1 \end{pmatrix} + \begin{pmatrix} \lambda_1 + |u_1|\lambda_2 \\ \lambda_1 + |u_2|\lambda_2 \\ \lambda_1 + |u_3|\lambda_2 \\ \lambda_2 \\ -\lambda_2 \end{pmatrix} + \begin{pmatrix} v_{s1} \\ v_{s2} \\ v_{s3} \\ 0 \\ 0 \end{pmatrix} \tag{2.13}$$

$$A^T \dot{q} = \begin{bmatrix} \dot{q}_{L_1} + \dot{q}_{L_2} + \dot{q}_{L_3} \\ |u_1|\dot{q}_{L_1} + |u_2|\dot{q}_{L_2} + |u_3|\dot{q}_{L_3} + \dot{q}_{C_1} - \dot{q}_{C_2} \end{bmatrix} = \begin{bmatrix} 0 \\ 0 \end{bmatrix} \tag{2.14}$$

Solving the vector equation (2.13) for λ_2 yields:

$$\lambda_2 = \frac{q_{C_1}}{C} \tag{2.15}$$

In the same way, adding up the upper three relationships in equation (2.13), and solving for λ_1, the following expression is obtained:

$$\lambda_1 = \frac{q_{C_1}}{3C}\left(\theta(-u_1)u_1 + \theta(-u_2)u_2 + \theta(-u_3)u_3\right) + \frac{q_{C_2}}{3C}\left(\theta(u_1)u_1 + \theta(u_2)u_2 + \theta(u_3)u_3\right) \tag{2.16}$$

Substituting the above expressions for λ_1 and λ_2 into equation (2.13), and after some simple manipulations, yields:

$$L\begin{pmatrix} \ddot{q}_{L_1} \\ \ddot{q}_{L_2} \\ \ddot{q}_{L_3} \end{pmatrix} = \frac{1}{3}\begin{bmatrix} -2 & 1 & 1 \\ 1 & -2 & 1 \\ 1 & 1 & -2 \end{bmatrix}\left[\frac{q_{C_1}}{C}\begin{pmatrix} \theta(-u_1)u_1 \\ \theta(-u_2)u_2 \\ \theta(-u_3)u_3 \end{pmatrix} + \frac{q_{C_2}}{C}\begin{pmatrix} \theta(u_1)u_1 \\ \theta(u_2)u_2 \\ \theta(u_3)u_3 \end{pmatrix}\right] + \begin{pmatrix} v_{s1} \\ v_{s2} \\ v_{s3} \end{pmatrix} \qquad (2.17)$$

Also, with the last relationship of equation (2.13), and using expression for λ_2 (2.15), the dynamics for the charge in the second capacitor can be stated as:

$$\dot{q}_{C_2} = \sum_{j=1}^{3} \dot{q}_{L_j}\, \theta(u_j)u_j - \frac{q_{C_1} + q_{C_2}}{RC} \qquad (2.18)$$

In the same way, substitution of equation (2.18) in the second relationship of equation (2.14) leads to the following expression, which describes the dynamics of the first capacitor:

$$\dot{q}_{C_1} = \sum_{j=1}^{3} \dot{q}_{L_j}\, \theta(-u_j)u_j - \frac{q_{C_1} + q_{C_2}}{RC} \qquad (2.19)$$

Summarizing, equations (2.17) to (2.19) fully describe the dynamics of the NPC–3 converter used as a rectifier, with u_1, u_2 and u_3 acting as the control inputs.

2.4 Coordinate transformations

To describe the system in a more natural way and to simplify the controller design, coordinate transformations will be applied to the previously proposed model represented by equations (2.17) to (2.19).

Notice from Figure 2.1 that the voltages v_1, v_2 and v_3 can be expressed as:

$$\begin{pmatrix} v_1 \\ v_2 \\ v_3 \end{pmatrix} = \frac{q_{C_1}}{C}\begin{pmatrix} \theta(-u_1)u_1 \\ \theta(-u_2)u_2 \\ \theta(-u_3)u_3 \end{pmatrix} + \frac{q_{C_2}}{C}\begin{pmatrix} \theta(u_1)u_1 \\ \theta(u_2)u_2 \\ \theta(u_3)u_3 \end{pmatrix} \qquad (2.20)$$

16

Therefore, equation (2.17) could be expressed in a simpler form if v_1, v_2 and v_3 are used as control inputs instead of the expression on the right hand side of equation (2.20).

Recalling some basic properties of the unit step function:

$$\theta(y)\theta(-y) = 0 \qquad\qquad \theta(y) + \theta(-y) = 1$$
$$\theta(y)\theta(y) = \theta(y) \qquad\qquad \theta(-y)\theta(-y) = \theta(-y)$$

And noticing, from Figure 2.5, that $\theta(v_i) = \theta(u_i)$, $i \in \{1,2,3\}$, then equation (2.20) can be solved for the control inputs u_1, u_2 and u_3 yielding:

$$\begin{pmatrix} u_1 \\ u_2 \\ u_3 \end{pmatrix} = \frac{C}{q_{C_1}}\begin{pmatrix} \theta(-v_1)v_1 \\ \theta(-v_2)v_2 \\ \theta(-v_3)v_3 \end{pmatrix} + \frac{C}{q_{C_2}}\begin{pmatrix} \theta(v_1)v_1 \\ \theta(v_2)v_2 \\ \theta(v_3)v_3 \end{pmatrix} \tag{2.21}$$

The i–th relationship in equation (2.20) is plot in Figure 2.5. Previous works [17] make use of quadratic polynomials to model such a switching stage, however, the authors assume that the voltage of the two capacitors are approximately equal at all times, therefore dropping the quadratic term. This provides a simpler, yet compromised, model. Here, no such assumption is necessary. It is also clear, that equations (2.20) and (2.21) are isomorphisms as long as q_{C_1}, q_{C_2} and C are different from zero.

Although expressions (2.20) and (2.21) can be derived from other equivalent modeling approaches, they do appear naturally as a consequence of the piecewise linear representation of the switching stage and the further Euler–Lagrange Formulation. One of the primary contributions of this work is the use of the isomorphism (2.20)–(2.21) to simplify the controller design while providing with a complete model for the NPC–3 inverter.
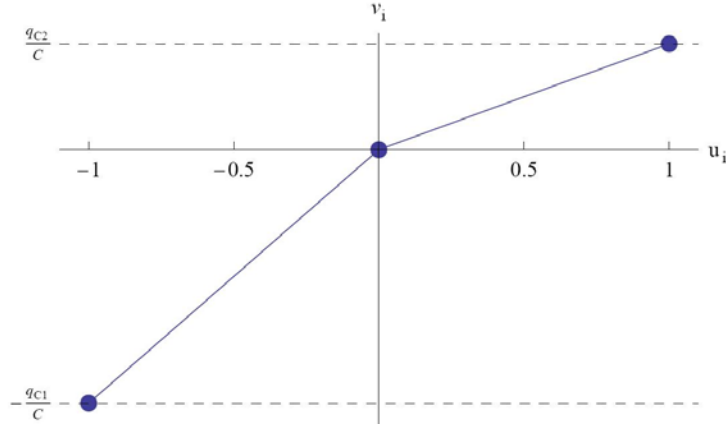
Figure 2.5 Voltage across the switching stage referred to the neutral point (0) as a function of the *i–th* control input u_i, $i \in \{1,2,3\}$. This relationship fits all three allowable points (black dots).

Substituting equation (2.20) in (2.17) gives the vector equation describing the dynamics of the currents in the inductors in a rather simpler form:

$$L\begin{pmatrix} \ddot{q}_{L_1} \\ \ddot{q}_{L_2} \\ \ddot{q}_{L_3} \end{pmatrix} = \begin{pmatrix} v_{s1} \\ v_{s2} \\ v_{s3} \end{pmatrix} - \frac{1}{3}\begin{bmatrix} 2 & -1 & -1 \\ -1 & 2 & -1 \\ -1 & -1 & 2 \end{bmatrix}\begin{pmatrix} v_1 \\ v_2 \\ v_3 \end{pmatrix} \tag{2.22}$$

As above, direct substitution of equation (2.20) in equations (2.18) and (2.19) leads to:

$$\dot{q}_{C_2} = \frac{C}{q_{C_2}} \sum_{j=1}^{3} \dot{q}_{L_j} \, \theta(v_j) v_j - \frac{q_{C_1}+q_{C_2}}{RC} \tag{2.23}$$

and

$$\dot{q}_{C_1} = \frac{C}{q_{C_1}} \sum_{j=1}^{3} \dot{q}_{L_j} \, \theta(-v_j) v_j - \frac{q_{C_1}+q_{C_2}}{RC} \tag{2.24}$$

Or alternatively, multiplying equations (2.23) and (2.24) by q_{C_2} and q_{C_1}, respectively, and after factorization of the time derivatives yields:

$$\frac{1}{2}\frac{d}{dt}\left(q_{C_2}^{\;2}\right) = C \sum_{j=1}^{3} \dot{q}_{L_j} \, \theta(v_j) v_j - q_{C_2}\left(\frac{q_{C_1}+q_{C_2}}{RC}\right) \tag{2.25}$$

18

and

$$\frac{1}{2}\frac{d}{dt}\left(q_{C_1}{}^2\right) = C\sum_{j=1}^{3} \dot{q}_{L_j}\,\theta\left(-v_j\right)v_j - q_{C_1}\left(\frac{q_{C_1}+q_{C_2}}{RC}\right) \qquad (2.26)$$

Notice that:

$$\sum_{j=1}^{3} \dot{q}_{L_j}\,\theta\left(v_j\right)v_j + \sum_{j=1}^{3} \dot{q}_{L_j}\,\theta\left(-v_j\right)v_j = \sum_{j=1}^{3} \dot{q}_{L_j}\left(\theta\left(v_j\right)+\theta\left(-v_j\right)\right)v_j = \sum_{j=1}^{3} \dot{q}_{L_j}v_j \qquad (2.27)$$

and

$$\sum_{j=1}^{3} \dot{q}_{L_j}\,\theta\left(-v_j\right)v_j - \sum_{j=1}^{3} \dot{q}_{L_j}\,\theta\left(v_j\right)v_j = \sum_{j=1}^{3} \dot{q}_{L_j}\left(\theta\left(-v_j\right)-\theta\left(v_j\right)\right)v_j = -\sum_{j=1}^{3} \dot{q}_{L_j}\left|v_j\right| \qquad (2.28)$$

Remark 2.2 Notice, from expressions (2.20) and (2.22) that, when the charge in both capacitors is zero, the inductor's currents and the source voltages have a 90º phase shift difference and the right hand side of equations (2.25) and (2.26) vanishes.

In order to reduce the complexity of the control inputs, equations (2.27)-(2.28) suggest as a natural selection for state variables the following non–isomorphic transformation:

$$\begin{bmatrix} \chi_1 \\ \chi_2 \\ \chi_3 \\ \chi_4 \\ \chi_5 \end{bmatrix} = \begin{bmatrix} \dot{q}_{L_1} \\ \dot{q}_{L_2} \\ \dot{q}_{L_3} \\ \dfrac{q_{C_1}{}^2 + q_{C_2}{}^2}{2C^2} \\ \dfrac{q_{C_1}{}^2 - q_{C_2}{}^2}{2C^2} \end{bmatrix}$$

This transformation has the drawback of allowing multiple undesired equilibria. To avoid such ambiguities the following similar, yet isomorphic, coordinate transformation is proposed:

$$
\begin{bmatrix} x_1 \\ x_2 \\ x_3 \\ x_4 \\ x_5 \end{bmatrix} = \begin{bmatrix} \dot{q}_{L_1} \\ \dot{q}_{L_2} \\ \dot{q}_{L_3} \\ \dfrac{q_{C_1}\left|q_{C_1}\right| + q_{C_2}\left|q_{C_2}\right|}{2C^2} \\ \dfrac{q_{C_1}\left|q_{C_1}\right| - q_{C_2}\left|q_{C_2}\right|}{2C^2} \end{bmatrix} \qquad (2.29)
$$

Given the fact that polarized electrolytic capacitors are the standard use in the dc link in power electronics systems, it is assumed that the voltages across them are nonnegative at all times. Restrictions $V_{C_1} \geq 0$ and $V_{C_2} \geq 0$, or equivalently $q_{C_1} \geq 0$ and $q_{C_2} \geq 0$, can be expressed in the new coordinates as:

$$
x_4{}^2 - x_5{}^2 \geq 0 \wedge x_4 \geq 0 \qquad (2.30)
$$

Notice from figure 2.6 that restriction (2.30) is not artificially included in the transformation, but it is a consequence of a physical restriction.
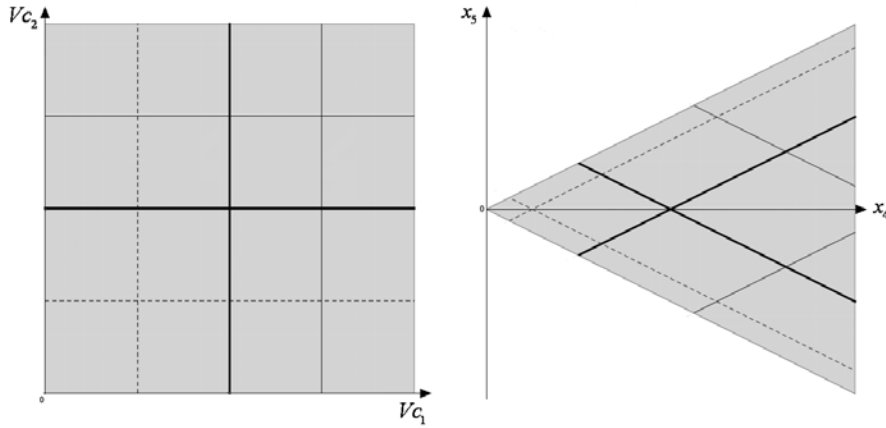

Figure 2.6 Graphical representation of the coordinate transformations. To provide with a clear view of the physical meaning of the transformation, the original coordinates have been used by means of the relationships $Vc_1 = \dfrac{q_{C_1}}{C}$ and $Vc_2 = \dfrac{q_{C_2}}{C}$. The thin, dashed and thick lines indicate various locations where either Vc_1 or Vc_2 are constant.

Remark 2.1 Coordinate transformation (2.29) allows for a more natural representation of the system model, where x_4 is proportional to the potential energy in the system, and x_5 is a measure of its unbalance in the capacitors.

Finally, the model represented by equations (2.22) to (2.24) can be expressed in these new coordinates as follows:

$$\dot{x}_{123} = \frac{1}{L}\left(v_{s123} - Bv_{123}\right) \tag{2.31}$$

$$\dot{x}_4 = \frac{1}{C}x_{123}^T v_{123} - \frac{4x_4}{RC} + \frac{2}{RC}\left(x_4 - \sqrt{x_4^2 - x_5^2}\right) \tag{2.32}$$

$$\dot{x}_5 = -\frac{1}{C}x_{123}^T v_{123} - \frac{2x_5}{RC} \tag{2.33}$$

where $x_{123} = \begin{pmatrix} x_1 \\ x_2 \\ x_3 \end{pmatrix}$, $v_{s123} = \begin{pmatrix} v_{s1} \\ v_{s2} \\ v_{s3} \end{pmatrix}$, $B = -\frac{1}{3}\begin{bmatrix} 2 & -1 & -1 \\ -1 & 2 & -1 \\ -1 & -1 & 2 \end{bmatrix}$, $v_{123} = \begin{pmatrix} v_1 \\ v_2 \\ v_3 \end{pmatrix}$

and $\upsilon_{123} \triangleq \begin{bmatrix} |v_1| & |v_2| & |v_3| \end{bmatrix}^T$

Consequently, voltages v_1, v_2 and v_3 can now be used to design the controller in an easier way and the actual control inputs u_i, $i \in \{1,2,3\}$ can be solved from v_1, v_2 and v_3 using equation (2.21).

2.5 Transformation to fixed frame or alpha–beta coordinates

To take advantage of the fact that no fourth wire is considered, and that the source voltages are assumed to be equilibrated, i.e., their sum is zero, one last coordinate

transformation will be applied to equations (2.31)-(2.33) to further reduce the model. For this purpose, consider the following Clarke's transformation:

$$T \triangleq \frac{2}{\sqrt{3}} \begin{bmatrix} 1 & -\dfrac{1}{2} & -\dfrac{1}{2} \\[2mm] 0 & \dfrac{\sqrt{3}}{2} & -\dfrac{\sqrt{3}}{2} \\[2mm] \dfrac{1}{\sqrt{2}} & \dfrac{1}{\sqrt{2}} & \dfrac{1}{\sqrt{2}} \end{bmatrix} \qquad (2.34)$$

which represents a linear map, so that:

$$\zeta_{\alpha\beta\gamma} = T\zeta_{123}, \quad \zeta_{123} = T^{-1}\zeta_{\alpha\beta\gamma} \quad \text{and} \quad T^{-1} = \frac{1}{2}T^{T} \qquad (2.35)$$

Therefore the coordinates transformations $\zeta_{123} \leftrightarrow \zeta_{\alpha\beta\gamma}$ for $\zeta \in \{x, v, v_s\}$ can be performed as follows:

$$\begin{pmatrix} \zeta_\alpha \\ \zeta_\beta \\ \zeta_\gamma \end{pmatrix} = \frac{1}{\sqrt{3}} \begin{bmatrix} (2\zeta_1 - \zeta_2 - \zeta_3) \\ \sqrt{3}(\zeta_2 - \zeta_3) \\ \sqrt{2}(\zeta_1 + \zeta_2 + \zeta_3) \end{bmatrix} \quad \text{and} \quad \begin{pmatrix} \zeta_1 \\ \zeta_2 \\ \zeta_3 \end{pmatrix} = \frac{1}{2\sqrt{3}} \begin{bmatrix} 2\zeta_\alpha + \sqrt{2}\zeta_\gamma \\ -\zeta_\alpha + \sqrt{3}\zeta_\beta + \sqrt{2}\zeta_\gamma \\ -\zeta_\alpha - \sqrt{3}\zeta_\beta + \sqrt{2}\zeta_\gamma \end{bmatrix} \qquad (2.36)$$

Using these transformations, the following vectors are defined:

$$\zeta_{\alpha\beta} = \begin{pmatrix} \zeta_\alpha \\ \zeta_\beta \end{pmatrix}, \qquad \text{and} \quad \zeta_{\alpha\beta\gamma} = \begin{pmatrix} \zeta_\alpha \\ \zeta_\beta \\ \zeta_\gamma \end{pmatrix}$$

Map (2.35) is of standard use in the power electronics literature and is commonly addressed as the conventional $1\ 2\ 3 \rightarrow \alpha\beta\gamma$ transformation as well. Consequently, equation (2.31) can be rewritten as:

$$L\begin{pmatrix} \dot{x}_\alpha \\ \dot{x}_\beta \\ 0 \end{pmatrix} = \begin{pmatrix} v_{s\alpha} \\ v_{s\beta} \\ 0 \end{pmatrix} - \begin{bmatrix} 1 & 0 & 0 \\ 0 & 1 & 0 \\ 0 & 0 & 0 \end{bmatrix} \begin{pmatrix} v_\alpha \\ v_\beta \\ v_\gamma \end{pmatrix} \qquad (2.37)$$

It is observed that, even though v_γ can be non–zero for the time being, it makes no contribution to the dynamics described in equation (2.37), hence the latter can be rewritten in matrix form as:

$$\dot{x}_{\alpha\beta} = \frac{1}{L}\left(v_{s\alpha\beta} - v_{\alpha\beta}\right) \tag{2.38}$$

where it has been taken the advantage of the fact that no fourth wire is considered ($x_\gamma = 0$) and that the source voltages are assumed to have no homopolar component ($v_{s\gamma} = 0$). In the same manner, using the $\alpha\beta\gamma$–coordinates, equations (2.32) and (2.33) are expressed as:

$$\dot{x}_4 = \frac{1}{2C}x_{\alpha\beta}^T v_{\alpha\beta} - \frac{4x_4}{RC} + \frac{2}{RC}\left(x_4 - \sqrt{x_4{}^2 - x_5{}^2}\right) \tag{2.39}$$

$$\dot{x}_5 = \frac{1}{2C}x_{\alpha\beta}^T \upsilon_{\alpha\beta} - \frac{2x_5}{RC} \tag{2.40}$$

where, $\quad \upsilon_{\alpha\beta} = \frac{1}{6}\left(\begin{array}{c} 2\sqrt{2}\left|\sqrt{2}v_\alpha + v_\gamma\right| - \left|v_\alpha + \sqrt{3}v_\beta - \sqrt{2}v_\gamma\right| - \left|v_\alpha - \sqrt{3}v_\beta - \sqrt{2}v_\gamma\right| \\ \sqrt{3}\left(\left|v_\alpha - \sqrt{3}v_\beta - \sqrt{2}v_\gamma\right| - \left|v_\alpha + \sqrt{3}v_\beta - \sqrt{2}v_\gamma\right|\right) \end{array} \right)$

Note here that, although $x_\gamma = 0$, no consideration is made about the nature of v_γ yet. This will be used in the next chapter, where under certain considerations, the transformation $1\,2\,3 \to \alpha\beta\gamma$ will actually map a 3 dimensional coordinate vector into a 2 dimensional one; becoming a $1\,2\,3 \to \alpha\beta$ transformation.

Summarizing, equations (2.38) through (2.40) fully describe the dynamics of the NPC–3 converter used as a synchronous rectifier and represent an adequate model suitable for control design purposes.

2.6 Control objectives

To ensure the highest possible power factor (closest to 1), the first objective consists in forcing the inductors' currents to follow references that are proportional to the corresponding source voltage signals, i.e., a *tracking* objective is established in the inductors' currents. The second and third objectives involve driving the charge of each capacitor to a desired constant reference value. In this work, the reference value is the same for both capacitors. Following the previously defined coordinate transformations for the capacitors' charges in equation (2.29), both objectives can be accomplished equivalently by driving the overall charge in the capacitors to a constant reference value, which is referred as the *regulation* objective; and then by zeroing their differences, which is referred as the *balance* objective.

All along this work the asterisk superscript (*) will be used to indicate a reference value or signal. Based on the previously defined model, the control objectives are listed next in a more formal way:

(i) *Tracking:* To force the inductors' currents to be proportional to the source voltage, a reference signal x^{*}_{123} is built. Therefore, the control objective can be stated as:

$$x_{123} \rightarrow x^{*}_{123}$$

$$\text{where} \quad x^{*}_{123} \rightarrow g_1 v_{s123} \quad \text{and} \quad \frac{d}{dt}(g_1) \rightarrow 0 \quad \text{as} \quad t \rightarrow \infty \tag{2.41}$$

here g_1 is a scalar yet to be defined representing an equivalent conductance observed by the source. Given that no fourth wire is being considered, the *tracking* objective can then be expressed in terms of alpha–beta coordinates as:

$$x_{\alpha\beta} \rightarrow x^{*}_{\alpha\beta} \tag{2.42}$$

24

where $x_{\alpha\beta}^* \to g_1 v s_{\alpha\beta}$ and $\dfrac{d}{dt}(g_1) \to 0$ as $t \to \infty$

Remark 2.3 As it will be noticed in the next chapter, the reference signal $x_{\alpha\beta}^*$ might not be proportional to the source voltages $v s_{\alpha\beta}$ at all times; that is, it may have transitory perturbations which vanish relatively fast.

(ii) *Regulation:* Consists in driving the overall charge of the capacitors towards a constant reference value, that is:

$$x_4 \to x_4^* \text{ as } t \to \infty, \quad \text{where} \quad x_4^* = V c_d^{\ 2} \qquad (2.43)$$

here $V c_d$ is the desired voltage level across the capacitors.

(iii) *Balance:* Consists in zeroing the differences of the capacitors' charges, that is:

$$x_5 \to x_5^* \text{ as } t \to \infty, \quad \text{where} \quad x_5^* = 0 \qquad (2.44)$$

Notice from equation (2.20) and Figure 2.5 that tracking can be performed if there is a minimum charge in the capacitors allowing a control action, even if the regulation or balance objectives have not been reached yet.

Controller Design

3.0 Introduction

In this chapter a controller for the NPC–3 converter is designed based on the model proposed in the previous chapter. First, the error dynamics model is used to locate the equilibrium point at the origin of the new coordinate system, and then a general overview of the strategy followed for the controller design is given. Later the Inner loop controller used to achieve the *tracking* objective is described. A constructive method is explained to introduce an extra control input in the form of a perturbation to the current reference signal which is one of the main contributions of the work. Amplitude modulation of the unperturbed reference signal is used to accomplish the *regulation* objective, whereas the introduced perturbation is employed as a control input to accomplish the *balance* objective. A stability analysis is performed, out of which, conditions involving system's parameters are established to preserve stability. Finally, an estimate of the region of attraction is calculated as well.

3.1 Error Dynamics

For the control design and for further stability analysis purposes, it is convenient to express the system (2.38)-(2.40) in terms of the state error dynamics with the error variables defined as follows:

$$\begin{pmatrix} \tilde{x}_\alpha \\ \tilde{x}_\beta \\ \tilde{x}_4 \\ \tilde{x}_5 \end{pmatrix} \triangleq \begin{pmatrix} x_\alpha \\ x_\beta \\ x_4 \\ x_5 \end{pmatrix} - \begin{pmatrix} x_\alpha^* \\ x_\beta^* \\ Vc_d{}^2 \\ 0 \end{pmatrix} \tag{3.1}$$

Based on these definitions, equations (2.38)-(2.40) can be rewritten as:

$$\dot{\tilde{x}}_{\alpha\beta} = \frac{1}{L}\left(v_{s\alpha\beta} - v_{\alpha\beta}\right) - \dot{x}_{\alpha\beta}^* \tag{3.2}$$

$$\dot{\tilde{x}}_4 = \frac{1}{2C} x_{\alpha\beta}^T v_{\alpha\beta} - \frac{4\left(\tilde{x}_4 + Vc_d{}^2\right)}{RC} + \frac{2}{RC}\left(\tilde{x}_4 + Vc_d{}^2 - \sqrt{\left(\tilde{x}_4 + Vc_d{}^2\right)^2 - \tilde{x}_5{}^2}\right) \tag{3.3}$$

$$\dot{\tilde{x}}_5 = \frac{1}{2C} x_{\alpha\beta}^T \upsilon_{\alpha\beta} - \frac{2\tilde{x}_5}{RC} \tag{3.4}$$

It easy to see that system (3.2)-(3.4) has its only equilibrium point located at the origin. Also, notice that the last term in equation (3.3) vanishes at the desired equilibrium point, this fact will be used for the stability analysis at the moment of proposing a candidate function following the Lyapunov approach.

3.2 Main assumptions

The control strategy will be constructed based upon the following 5 assumptions:

A1. **(Modulation)** It will be assumed that the use of a multicarrier phase–shifted modulation algorithm at a relatively high switching frequency as described in [14] makes no significant contribution to the model represented by equations (3.2)-(3.4). This imposes a restriction to the overall dynamics of the system: all system dynamics should be bandwidth–limited to at least one decade below the switching frequency of the IGBT devices.

A2. **(Decoupling assumption)** It is assumed that the dynamics of $\tilde{x}_{\alpha\beta}$ is much faster (at least one decade) than the dynamics of $\tilde{x}_4$. Also, the dynamics of $\tilde{x}_4$ is assumed to be much faster (around one decade) than the dynamics of $\tilde{x}_5$. Therefore control objectives can be scheduled to be reached accordingly following a time scale separation principle.

This assumption, on the one hand, facilitates de controller design, but on the other hand, it introduces certain limitations. Basically, time scale separation allows for a split controller design, that is, the controller can be designed to fulfill the control objectives separately and in cascade form. Evidently, perturbance rejection associated to the "fast" dynamics can be performed in an easier manner. However, *regulation* and *balance* controllers must be band limited; therefore, compromising the frequency response of the converter to load changes.

A3. **(Source voltages)** To facilitate the controller design, it is assumed that the source voltage $v_{s\alpha\beta}$ is a balanced sinusoidal signal of a known fundamental frequency ω. The signal amplitude is assumed to be constant or slowly varying.

A4. **(System parameters)** It is intended to design a robust controller with respect to parameter uncertainties. For that purpose, unless otherwise stated, system parameters R, L and C are assumed to be uncertain positive scalars, possibly changing in steps or that can be slowly varying.

A5. **(No homopolar component)** Given that no fourth wire is connected, no homopolar component is considered. Therefore, it is assumed that $x_\gamma = 0$ and $v_{s\gamma} = 0$, i.e. both voltages and currents are equilibrated. Moreover, the currents can still be unbalanced.

3.3 Overall description of the control strategy

To achieve the control objectives depicted in section 2.6, the control design is based on a time scale separation principle. Hence, control can be designed individually for each of the following three loops: *tracking, regulation and balance.* For that purpose, a four steps strategy is proposed:

1) The first objective — *tracking* — is intended to be completed quite rapidly. To fulfill this objective, a control vector $v_{\alpha\beta}$ is designed using a passivity based control (PBC) and a bank of resonant filters tuned at the harmonics of interest (odd) for harmonic compensation as described in [18].

2) Assuming that the currents have already reached its reference value $x_{\alpha\beta}^*$ in a relatively short time, equations (3.3) and (3.4) are averaged in order to use its DC components only. It is assumed that the harmonic components cause a small ripple in the overall response of x_4 and x_5 only.

3) A current reference signal $x_{\alpha\beta}^*$ is built in such a way that it includes extra terms that serve as control inputs. This is achieved by adding a transitory perturbation to the intended final reference signal.

4) Finally, using the introduced extra control inputs in equations (3.3) and (3.4), the second and third objectives –*regulation* and *balance*– , respectively, can be soon after reached.

3.4 Inner loop: *current tracking*

To solve the *tracking* objective, the control input $v_{\alpha\beta}$ is designed following a similar procedure to the one used in [19]. This control law is based in the energy shaping plus damping injection methodology of the PBC [20]. The process consists in, first, make a copy of the subsystem representing the current dynamics and evaluate it at

the desired current reference. Second, add the required damping term. Out of this, the following expression is obtained:

$$L\frac{d}{dt}\left(x^*_{\alpha\beta}\right)=v_{s\alpha\beta}-v_{\alpha\beta}-L\frac{d}{dt}\left(\tilde{x}_{\alpha\beta}\right)+k_1\tilde{x}_{\alpha\beta} \tag{3.5}$$

solving system (3.5) for $v_{\alpha\beta}$ yields the following control law:

$$v_{\alpha\beta}=v_{s\alpha\beta}+k_1\tilde{x}_{\alpha\beta}+\phi$$

where $\phi=-L\frac{d}{dt}\left(x_{\alpha\beta}\right)$ represents an unknown periodic disturbance.

To compensate the periodic disturbance ϕ, a method based in the Internal Model Principle [21] is followed. This technique consists in the introduction of a bank of resonant filters tuned at the harmonics under compensation (see [18] and the references therein for further details) to compensate for such a periodic disturbance. In this case the following controller for the current tracking loop is proposed:

$$v_{\alpha\beta}=vs_{\alpha\beta}+k_1\,\tilde{x}_{\alpha\beta}+\sum_{k\in H}\frac{2\gamma_k s}{s^2+k^2w^2}\tilde{x}_{\alpha\beta} \tag{3.6}$$

where γ_k, $\forall k\in H$, are positive design parameters, where $H=\{1,3,\cdots\}$, i.e., the odd harmonics are compensated, and s is the Laplace complex variable. Figure 3.1 depicts a block diagram for the proposed controller in (3.6)
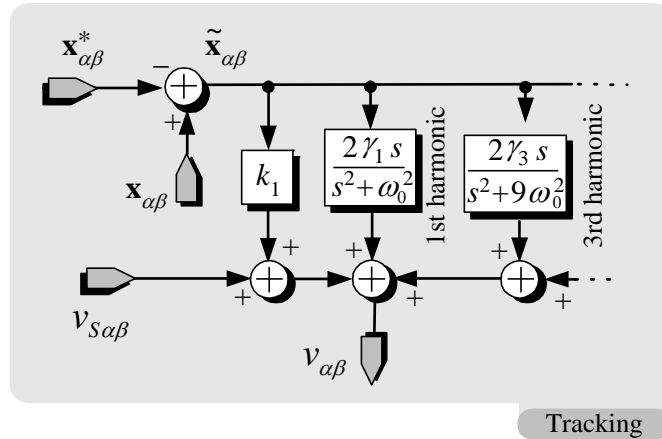

Figure 3.1 Block diagram of the proposed controller for the tracking loop.

31

3.5 Averaging of the charge dynamics equations

Notice that the first term on the right hand side of equations (3.3) and (3.4) could contain, in general, products of periodic signals producing an unavoidable ripple in the overall response of x_4 and x_5. Consequently, control objectives (2.43) and (2.44) could only be accomplished in average. For that purpose, the following averaging operator is defined (also referred as moving average):

$$[\cdot]_{DC} = \frac{\omega}{2\pi} \int_{\tau-\pi/\omega}^{\tau+\pi/\omega} (\cdot)\, dt$$

For a periodical signal of angular frequency ω, or its harmonics, the operator $[\cdot]_{DC}$ will calculate the constant term of its Fourier series expansion. Direct application of this operator to equations (3.3) and (3.4) yields:

$$\dot{z}_4 = \left[\frac{1}{2C} x_{\alpha\beta}^{T} v_{\alpha\beta}\right]_{DC} - \frac{4\left(z_4 + Vc_d{}^2\right)}{RC} + \frac{2}{RC}\left(z_4 + Vc_d{}^2 - \sqrt{\left(z_4 + Vc_d{}^2\right)^2 - z_5{}^2}\right) \qquad (3.7)$$

$$\dot{z}_5 = \left[\frac{1}{2C} x_{\alpha\beta}^{T} v_{\alpha\beta}\right]_{DC} - \frac{2z_5}{RC} \qquad (3.8)$$

where for simplicity, the following new *averaged* coordinates are introduced:

$$z_4 = \left[\tilde{x}_4\right]_{DC} \quad \text{and} \quad z_5 = \left[\tilde{x}_5\right]_{DC}$$

3.6 Design of the current reference signal

Following a similar ideas as the ones used in [19], a transitory perturbation $g_2\psi_{\alpha\beta}$ will be added to the intended final current reference signal $g_1 v s_{\alpha\beta}$ as follows:

$$x_{\alpha\beta}^{*} = g_1 v s_{\alpha\beta} + g_2 \psi_{\alpha\beta} \qquad (3.9)$$

The idea behind this modification is to introduce an extra control input that will be used later on to solve the balance issue. In what follows **A3** is appealed, and also it is assumed that the source voltages are balanced and, therefore, they can be expressed as:

$$vs_{\alpha\beta} = \sqrt{2}\,V_{rms}\begin{pmatrix} sin(\omega t) \\ -cos(\omega t) \end{pmatrix} \tag{3.10}$$

where V_{rms} is the *line–to–line RMS* voltage of the power sources. Also it is assumed that $\psi_{\alpha\beta}$ is composed by periodic signals of the known fundamental frequency ω, and possibly by higher order harmonics. Therefore, the reference signal can be expressed as:

$$x_{\alpha\beta}^* = g_1 vs_{\alpha\beta} + g_2\begin{pmatrix} B_1\, sin(m\omega t + \phi_1) \\ B_2\, sin(n\omega t + \phi_2) \end{pmatrix} \tag{3.11}$$

Following the time scale separation principle, it is assumed that the *tracking* objective has been reached at this point, i.e., $x_{\alpha\beta} = x_{\alpha\beta}^*$. Therefore, making $\tilde{x}_{\alpha\beta} = 0$, so the proposed controller in (3.6) becomes $v_{\alpha\beta} = vs_{\alpha\beta}$. Choosing for simplicity $v_\gamma = 0$, the expressions inside the averaging operator in (3.7) and (3.8) can be calculated as follows:

$$\left[\frac{1}{2C}x_{\alpha\beta}^T v_{\alpha\beta}\right]_{DC} = \left[\frac{g_1 V_{rms}^2}{C} + \frac{g_2 V_{rms}}{\sqrt{2}\,C}B_1\, sin(\omega t)sin(\phi_1 + m\omega t)\right]_{DC} -$$

$$\left[\frac{g_2 V_{rms}}{\sqrt{2}\,C}B_2\, cos(\omega t)sin(\phi_2 + n\omega t)\right]_{DC} \tag{3.12}$$

$$= \frac{g_1 V_{rms}^2}{C} + \frac{g_2 V_{rms}}{\sqrt{2}\,C\,\pi}\left(B_1\, cos(\phi_1)\frac{sin(m\pi)}{1-m^2} + B_2\, sin(\phi_2)\frac{n\,sin(n\pi)}{n^2-1}\right)$$

and

$$\left[\frac{1}{2C} x_{\alpha\beta}^{T} \upsilon_{\alpha\beta}\right]_{DC} =$$

$$\left[\frac{\sqrt{2}\, g_2\, V_{rms}}{12\,C}\left(4\,B_1\, \left|sin\left(\omega t\right)\right|\, sin\left(\phi_1 + m\,\omega t\right)-\right.\right.$$

$$\left|\sqrt{3}\, cos\left(\omega t\right)+ sin\left(\omega t\right)\right|\left(B_1\, sin\left(\phi_1 + m\,\omega t\right)-\sqrt{3}\, B_2\, sin\left(\phi_2 + n\,\omega t\right)\right)-$$

$$\left|-\sqrt{3}\, cos\left(\omega t\right)+ sin\left(\omega t\right)\right|\left(B_1\, sin\left(\phi_1 + m\,\omega t\right)+\sqrt{3}\, B_2\, sin\left(\phi_2 + n\,\omega t\right)\right)\right)+$$

$$\frac{g_1\, V_{rms}^{\ 2}}{6\,C}\left(4\, \left|sin\left(\omega t\right)\right|\, sin\left(\omega t\right)-\right.$$

$$\left|-\sqrt{3}\, cos\left(\omega t\right)+ sin\left(\omega t\right)\right|\left(-\sqrt{3}\, cos\left(\omega t\right)+ sin\left(\omega t\right)\right)-$$

$$\left.\left|\sqrt{3}\, cos\left(\omega t\right)+ sin\left(\omega t\right)\right|\left(\sqrt{3}\, cos\left(\omega t\right)+ sin\left(\omega t\right)\right)\right)\right]_{DC}$$

applying the averaging operator the previous expression is expressed as:

$$\left[\frac{1}{2C} x_{\alpha\beta}^{T} \upsilon_{\alpha\beta}\right]_{DC} = \frac{\sqrt{2}\, g_2\, V_{rms}}{6\,C\,\pi}$$

$$\left(B_1\, sin\left(\phi_1\right)\frac{\left(\sqrt{3}\,m\left(1+2\,cos\left(\dfrac{m\,\pi}{3}\right)\right)-4\,sin\left(\dfrac{m\,\pi}{3}\right)\right)\left(sin\left(\dfrac{m\,\pi}{3}\right)- sin\left(\dfrac{2\,m\,\pi}{3}\right)\right)}{m^2 -1}+\right.$$

$$\left.\sqrt{3}\, B_2\, cos\left(\phi_2\right)\frac{\left(1-2\,cos\left(\dfrac{n\,\pi}{3}\right)\right)^2\, sin\left(\dfrac{n\,\pi}{3}\right)}{n^2 -1}\right)$$

(3.13)

Notice that both g_1 and g_2 appear in equation (3.12), whereas g_2 is present in (3.13) only. Consequently, careful selection of the involved parameters B_1, B_2, m, n, ϕ_1 and ϕ_2 is used to nullify the term containing g_2 on equation (3.12) without zeroing the right–hand side of equation (3.13). This can be achieved by choosing $B_1 = 0$, $B_2 = -1$, $n = 2$ and $\phi_2 = 0$. Using this selection of parameters, equation (3.11) becomes:

$$x_{\alpha\beta}^{*} = g_1 v s_{\alpha\beta} - g_2 \begin{pmatrix} 0 \\ sin(2\omega t) \end{pmatrix} \tag{3.14}$$

Choosing g_2 to be a scalar variable yet to be defined such that $\dot{g}_2 \to 0$ and $g_2 \to 0$ as $t \to \infty$, expression $g_2 \psi_{\alpha\beta}$ in equation (3.9) can be considered as a vanishing perturbation. At the same time $\psi_{\alpha\beta}$ is considered to be composed only by a second harmonic.

Using (3.10), expression (3.14) can be rewritten as:

$$x_{\alpha\beta}^{*} = g_1 v s_{\alpha\beta} + \frac{g_2}{V_{rms}^2} \begin{pmatrix} 0 \\ v_{s\alpha} \ v_{s\beta} \end{pmatrix} \tag{3.15}$$

Summarizing, equations (3.7) and (3.8) can be expressed as:

$$\dot{z}_4 = \frac{g_1 V_{rms}^2}{C} - \frac{4\left(z_4 + V c_d^{\ 2}\right)}{RC} + \frac{2}{RC}\left(z_4 + V c_d^{\ 2} - \sqrt{\left(z_4 + V c_d^{\ 2}\right)^2 - z_5^{\ 2}} \right) \tag{3.16}$$

$$\dot{z}_5 = -\frac{\sqrt{2}\, g_2 V_{rms}}{3C\pi} - \frac{2 z_5}{RC} \tag{3.17}$$

For large resistive loads i.e. $R \to \infty$, equations (3.16) and (3.17) become:

$$\dot{z}_4 = \frac{g_1 V_{rms}^2}{C}$$

$$\dot{z}_5 = -\frac{\sqrt{2}\, g_2 V_{rms}}{3C\pi}$$

Notice that the control inputs g_1 and g_2 provide the required damping so both objectives, *regulation* and *balance,* can be achieved even in case of no load presence. In section 3.8, detailed results are provided regarding the stability of the overall system, and conditions for particular circumstances can easily be derived from them.

3.7 Outer loop: *regulation* and *balance*

In what follows, g_1 and g_2 are designed to drive variables z_4 and z_5 to the origin. To avoid numerical errors, the following transformations on the control inputs are introduced:

$$G_1 = \frac{g_1 V_{rms}^2}{C} \quad \text{and} \quad G_2 = \frac{\sqrt{2}\, g_2 V_{rms}}{3 C \pi}$$

Substituting these expressions in equations (3.16) and (3.17) and evaluating at the equilibrium point, yields:

$$\dot{z}_4 \big|_0 = G_1 - \frac{4 V c_d^2}{R C}$$

$$\dot{z}_5 \big|_0 = - G_2$$

Therefore, G_1 can be calculated using a PI controller on z_4 so that the final value of $\frac{4 V c_d^2}{R C}$ is reached. Conversely, G_2 requires only a proportional controller on z_5.

Therefore, the following controllers are proposed:

$$G_1 = -k_{p1} z_4 - k_{i1} x_6 \quad \text{and} \quad G_2 = k_{p2} z_5$$

where $\dot{x}_6 = z_4$; and k_{p1}, k_{i1} and k_{p2} are positive constant scalar design parameters

To be consistent with the previously defined coordinates, and to keep the equilibrium point at the origin of the z coordinates, the following definition is made:

36

$$z_6 \triangleq x_6 + \frac{4Vc_d{}^2}{RC\,k_{i1}}$$

As a result, the closed loop system is expressed as:

$$\dot{z}_4 = -\left(k_{p1} + \frac{4}{RC}\right)z_4 - k_{i1}\,z_6 + \frac{2}{RC}\left(z_4 + Vc_d{}^2 - \sqrt{\left(z_4 + Vc_d{}^2\right)^2 - z_5{}^2}\right) \qquad (3.18)$$

$$\dot{z}_5 = -\left(k_{p2} + \frac{2}{RC}\right)z_5 \qquad (3.19)$$

$$\dot{z}_6 = z_4 \qquad (3.20)$$

where it is clear that the origin is the only equilibrium point of the averaged system.

The block diagram of the overall controller is shown in Figure 3.2. Notice, from the *Control inputs transformations* block (bottom block), that the control inputs $u_i, i \in \{1,2,3\}$ require that both Vc_1 and Vc_2 be non zero to be well defined. Thus, before any control action can be applied, a preload operation must be performed in such a way that capacitors voltages are drawn away form zero. A numerical example in Chapter 4 will show further details on this issue.
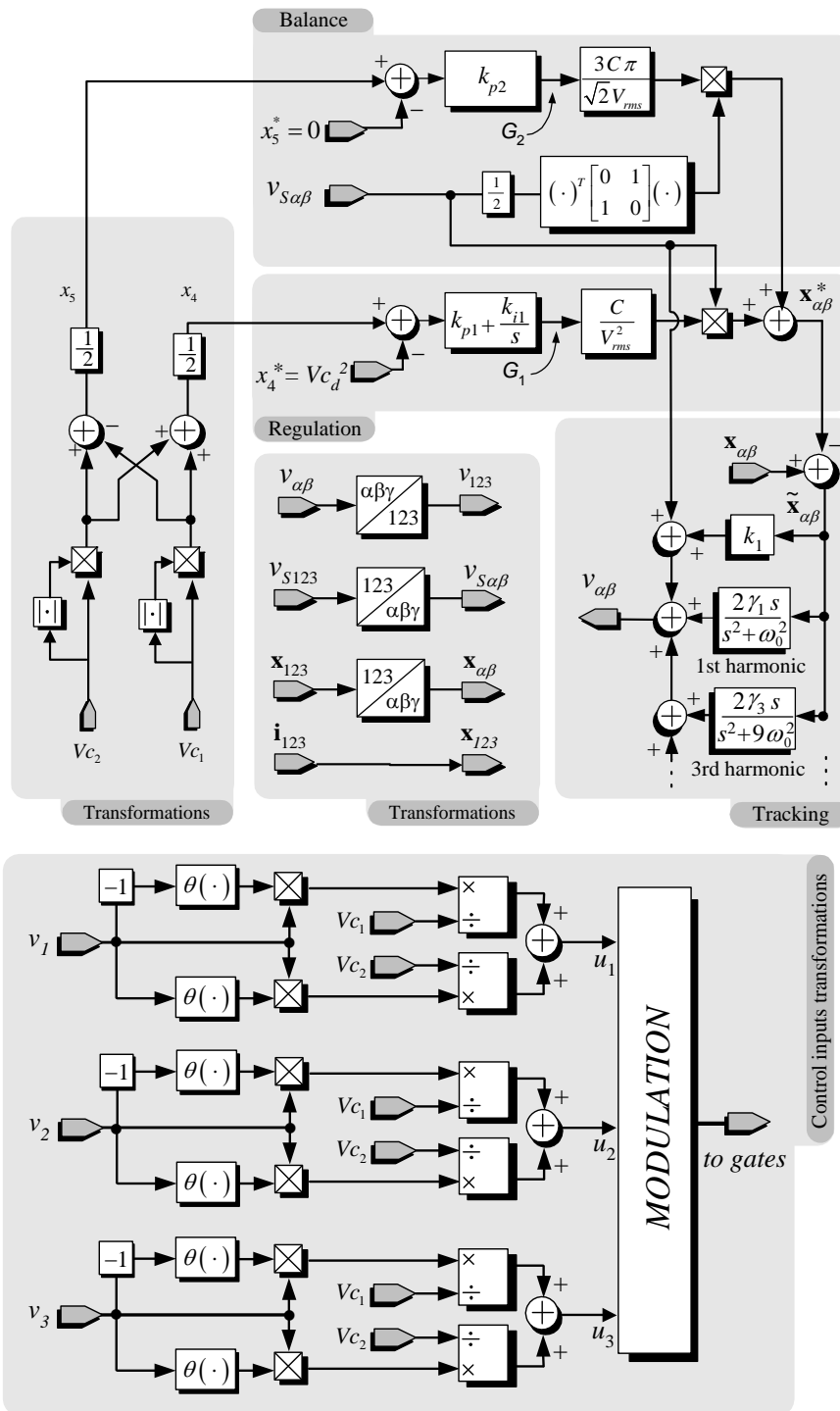
Figure 3.2 Flow Diagram for the proposed controller including both inner and outer loops as well as the transformations used.

3.8 Stability Analysis

Stability for the controllers proposed in section 3.4 and 3.7 can be studied in two stages following the aforementioned time scale separation principle. Stability of the current *tracking* loop can be found in [18]. On the other hand, stability in the sense of Lyapunov will be studied following a procedure described in [22] for the origin of the closed loop system (3.18) to (3.20).

Notice that the averaged system (3.18) though (3.20) can be expressed as:

$$
\begin{bmatrix} \dot{z}_4 \\ \dot{z}_5 \\ \dot{z}_6 \end{bmatrix} = - \begin{bmatrix} k_{p1} + \dfrac{4}{CR} & 0 & k_{i1} \\ 0 & k_{p2} + \dfrac{2}{CR} & 0 \\ -1 & 0 & 0 \end{bmatrix} \begin{bmatrix} z_4 \\ z_5 \\ z_6 \end{bmatrix} + \dfrac{2}{CR} \begin{bmatrix} Vc_d{}^2 + z_4 - \sqrt{\left(Vc_d{}^2 + z_4\right)^2 - z_5{}^2} \\ 0 \\ 0 \end{bmatrix} \qquad (3.22)
$$

Thus, separating the linear and nonlinear contributions to the charge dynamics equations, where it has been defined:

$$
A \triangleq \begin{bmatrix} -\left(k_{p1} + \dfrac{4}{CR}\right) & 0 & -k_{i1} \\ 0 & -\left(k_{p2} + \dfrac{2}{CR}\right) & 0 \\ 1 & 0 & 0 \end{bmatrix} \quad \text{and} \quad h(z) \triangleq \begin{bmatrix} \varphi \\ 0 \\ 0 \end{bmatrix} \quad \text{with}
$$

$$
\varphi \triangleq \dfrac{2}{CR}\left(Vc_d{}^2 + z_4 - \sqrt{\left(Vc_d{}^2 + z_4\right)^2 - z_5{}^2}\right)
$$

Equation (3.22) can be expressed in a much simpler way as:

$$
\dot{z} = A z + h(z) \qquad (3.23)
$$

Remark 3.1 Notice here that the matrix A corresponds to the Jacobian matrix of system (3.22) evaluated at the origin. Also, note, that all eigenvalues of A have negative real part:

$$eig_1(A) = -\left(k_{p2} + \frac{2}{RC}\right)$$

$$eig_2(A) = \frac{-RC\,k_{p1} - 4 - \sqrt{\left(RC\,k_{p1} + 4\right)^2 - 4R^2C^2k_{i1}}}{2RC}$$

$$eig_3(A) = \frac{-\left(RC\,k_{p1} + 4\right) + \sqrt{\left(RC\,k_{p1} + 4\right)^2 - 4R^2C^2k_{i1}}}{2RC}$$

Therefore, A is Hurwitz.

Remark 3.2 At this point it is convenient to notice that the physical restriction described in (2.30) can be expressed in the averaged coordinates z as:

$$\left(z_4 + Vc_d^2\right)^2 - z_5^2 \geq 0 \ \wedge\ z_4 + Vc_d^2 \geq 0 \tag{3.24}$$

Then, system (3.23) is defined in $D = \left\{(z_4, z_5, z_6) \,|\, \left(z_4 + Vc_d^2\right)^2 - z_5^2 > 0 \ \wedge\ z_4 > -Vc_d^2\right\}$.

Again, note that restriction (3.24) is not artificial but has a physical meaning due to the use of electrolytic capacitors.

Remark 3.3 System (3.23) can be considered as a perturbation of a nominal unperturbed linear system:

$$\dot{z} = A\,z \tag{3.25}$$

Also noticing that $h(0) = 0$, $h(z)$ can be considered as a vanishing perturbation. Therefore, following [22] a Lyapunov function for the unperturbed system (3.25) will be used as a candidate Lyapunov function for the perturbed system (3.23).

Remark 3.4 Note from the above definition of φ and from remark 3.2 that $\varphi \geq 0$ $\forall z \in D$. Therefore the following relationship holds:

$$\left\|h(z)\right\|_2 = \varphi, \ \forall z \in D$$

Considering remark 3.1, a Lyapunov function $V = z^T P z$ for the unperturbed system (3.25) can be derived after solving the following Lyapunov equation for P:

$$P A + A^T P = -I_3$$

where I_3 is the 3x3 identity matrix. This yields

$$P = \begin{pmatrix} \dfrac{RC(1+k_{i1})}{2k_{i1}(4+RCk_{p1})} & 0 & \dfrac{1}{2k_{i1}} \\[3ex] 0 & \dfrac{RC}{2(2+RCk_{p2})} & 0 \\[3ex] \dfrac{1}{2k_{i1}} & 0 & \dfrac{16+8RCk_{p1}+R^2C^2\left(k_{i1}+k_{i1}^2+k_{p1}^2\right)}{2RCk_{i1}(4+RCk_{p1})} \end{pmatrix}$$

Hence, following remark 3.3, the next Lyapunov candidate function is proposed for the perturbed system (3.23):

$$V = z^T P z$$

$$V = \frac{RC(1+k_{i1})z_4^2}{2k_{i1}(4+RCk_{p1})} + \frac{RC z_5^2}{4+2RCk_{p2}} + \frac{z_4 z_6}{k_{i1}} + \frac{16+RC\left(8k_{p1}+RC\left(k_{i1}+k_{i1}^2+k_{p1}^2\right)\right)z_6^2}{2RCk_{i1}(4+RCk_{p1})} \quad (3.26)$$

Derivation of V along the system's trajectories yields:

$$\dot{V} = -\|z\|_2^2 + \frac{2}{CR}\left(\frac{RC(1+k_{i1})z_4}{(4+RCk_{p1})k_{i1}} + \frac{z_6}{k_{i1}}\right)\left(Vc_d^2 + z_4 - \sqrt{\left(Vc_d^2+z_4\right)^2 - z_5^2}\right) \quad (3.27)$$

Hence, parameters k_{p1}, k_{i1} and k_{p2} can now be chosen to grant $\dot{V} < 0$ in some subdomain of D. Consequently, an upper bound for (3.27) can be obtained as:

$$\dot{V} = -\|z\|_2^2 + 2z^T P h(z)$$

$$= -\|z\|_2^2 + \varphi\left(\frac{RC(1+k_{i1})z_4}{(4+RCk_{p1})k_{i1}} + \frac{z_6}{k_{i1}}\right)$$

$$\leq -\|z\|_2^2 + \varphi\left(\frac{4+RC(1+k_{i1}+k_{p1})}{k_{i1}(4+RCk_{p1})}\right)\|z\|_2 \quad (3.28)$$

Following remark 3.4, $\dot{V}$ will be negative definite for some subdomain of D where $\|h(z)\|_2$ is bounded by the states, so that:

$$\|h(z)\|_2 < \gamma\|z\|_2 \quad \text{where} \quad \gamma = \frac{k_{i1}\left(4+RCk_{p1}\right)}{4+RC\left(1+k_{i1}+k_{p1}\right)}$$

To obtain a less conservative bound, it is pointed out that $h(z)$ is a *structured perturbation* [22], in the sense that its second and third components are identically zero at all times. Therefore, taking into account the full structure of perturbation $h(z)$, expression (3.28) can be rewritten as:

$$\dot{V} \le \left(\left(\frac{8+2RC\left(1+k_{i1}+k_{p1}\right)}{k_{i1}RC\left(4+RCk_{p1}\right)}\right)\left(Vc_d^{\ 2}+z_4-\sqrt{\left(z_4+Vc_d^{\ 2}\right)^2-z_5^{\ 2}}\right)-\|z\|_2\right)\|z\|_2$$

$$\le \left(\frac{8+2RC\left(1+k_{i1}+k_{p1}\right)}{k_{i1}RC\left(4+RCk_{p1}\right)}\left(\sqrt{\left(z_4+Vc_d^{\ 2}\right)^2}-\sqrt{\left(z_4+Vc_d^{\ 2}\right)^2-z_5^{\ 2}}\right)-\|z\|_2\right)\|z\|_2$$

$$\le \left(\frac{8+2RC\left(1+k_{i1}+k_{p1}\right)}{k_{i1}RC\left(4+RCk_{p1}\right)}\sqrt{z_5^{\ 2}}-\|z\|_2\right)\|z\|_2$$

$$\le \left(\frac{8+2RC\left(1+k_{i1}+k_{p1}\right)}{k_{i1}RC\left(4+RCk_{p1}\right)}\|z\|_2-\|z\|_2\right)\|z\|_2$$

$$\le \left(\frac{8+2RC\left(1+k_{i1}+k_{p1}\right)}{k_{i1}RC\left(4+RCk_{p1}\right)}-1\right)\|z\|_2^2$$

Hence, to assure negative definiteness of $\dot{V}$, a sufficiency condition can be established on the parameters R, C, k_{p1} and k_{i1} as:

$$\frac{8+2RC\left(1+k_{i1}+k_{p1}\right)}{k_{i1}RC\left(4+RCk_{p1}\right)} < 1$$

or alternatively:

$$k_{p1}k_{i1}(RC)^2 - 2(1 - k_{i1} + k_{p1})RC - 8 > 0 \qquad (3.29)$$

Finally, (3.26) represents a Lyapunov function for system (3.22) $\forall z \in D$ as long as condition (3.29) is met.

To obtain a maximal Lyapunov surface, the extrema of (3.26) are calculated on the boundary of D. A maximal Lyapunov function should be tangent to this boundary, so a minimum value for V on D is seek out. Calculation of the critical point of V on $(z_4 + Vc_d^2)^2 - z_5^2 = 0$, yields:

$$z_{4c} = \frac{(4 + CRk_{p1})(16 + 8CRk_{p1} + C^2R^2(k_{i1} + k_{i1}^2 + k_{p1}^2))Vc_d^2}{d} \quad \text{and}$$

$$z_{6c} = \frac{CR(4 + CRk_{p1})^2 Vc_d^2}{d}$$

where

$$d = 96 + 16CR(4k_{p1} + k_{p2}) + 2C^2R^2(1 + 4k_{i1} + 3k_{i1}^2 + 7k_{p1}^2 + 4k_{p1}k_{p2})$$
$$+ C^3R^3(k_{p1}^3 + k_{p2} + k_{p1}^2 k_{p2} + k_{i1}^2(k_{p1} + k_{p2}) + k_{i1}(k_{p1} + 2k_{p2}))$$

Let

$$\begin{bmatrix} \dfrac{\partial^2 V}{\partial z_4^2} & \dfrac{\partial^2 V}{\partial z_4 \partial z_5} \\[2mm] \dfrac{\partial^2 V}{\partial z_5 \partial z_4} & \dfrac{\partial^2 V}{\partial z_5^2} \end{bmatrix} = \begin{bmatrix} RC\left(\dfrac{1 + k_{i1}}{k_{i1}(4 + RCk_{p1})} + \dfrac{1}{2 + RCk_{p2}}\right) & \dfrac{1}{k_{i1}} \\[4mm] \dfrac{1}{k_{i1}} & \dfrac{16 + RC(8k_{p1} + RC(k_{i1} + k_{i1}^2 + k_{p1}^2))}{RCk_{i1}(4 + RCk_{p1})} \end{bmatrix}$$

be the Hessian matrix for V, and $\Delta = \dfrac{d}{k_{i1}(4 + RCk_{p1})^2(2 + RCk_{p2})}$ its

determinant. Since $\dfrac{\partial^2 V}{\partial z_4^2} > 0$ and $\Delta > 0$, evaluating V at its critical point gives the minimum value:

$$V = \frac{RCVc_d^4(16 + 8 + RCk_{p1} + R^2C^2(1 + 2k_{i1} + k_{i1}^2 + k_{p1}^2))}{2d} \qquad (3.30)$$

Therefore, choosing:

$$c = \frac{RCVc_d^4\left(16 + 8RCk_{p1} + R^2C^2\left(1 + 2k_{i1} + k_{i1}^2 + k_{p1}^2\right)\right)}{2d}$$

$V - c = 0$ is a maximal Lyapunov surface and following [22], it can be concluded that $\Omega_c \triangleq \left\{z \in \mathbb{R}^3 \middle| V(z) \le c\right\}$ is bounded and contained in D. Hence, every trajectory starting in Ω_c remains in Ω_c approaching the origin as $t \to \infty$, as long as condition (3.29) is met.

It can be concluded that the origin of the averaged system (3.22) is an asymptotically stable equilibrium point, as long as condition (3.29) is met.

Finally, it is interesting to point out that under the assumption that both capacitors have reached their reference values ($z_4 = 0$ and $z_5 = 0$) and setting the initial of the integrator x_6 to zero, solution of $V - c = 0$ for R, provides with the maximum load the converter can handle so that initial conditions still remain in the region of attraction.

$$\frac{RCVc_d^4\left(16 + 8RCk_{p1} + R^2C^2\left(1 + 2k_{i1} + k_{i1}^2 + k_{p1}^2\right)\right)}{2d} =$$

$$\frac{16 + RC\left(8k_{p1} + RC\left(k_{i1} + k_{i1}^2 + k_{p1}^2\right)\right)}{2RCk_{i1}\left(4 + RCk_{p1}\right)}\left(\frac{4Vc_d^2}{RCk_{i1}}\right)^2$$

Chapter 4

Numerical Results

4.0 Introduction

Simulations of the NPC–3 converter used as a synchronous rectifier along with the controller proposed in sections 3.4 and 3.7 were performed using the commercially available software PSCAD®/EMTDC™ 4.0. This is a widely spread engineering tool for the design and verification of power systems. The topology presented in Figure 2.1 was recreated using the parameters shown in table 4.1

$$\omega = 120\,\pi \text{ rad/sec } (f = 60\,Hz)$$

$$L = 3\,mH$$

$$C = 2200\,\mu F$$

$$R = 100\Omega,\ 23\Omega$$

$$V_{rms} = 220V \text{ (\emph{RMS, line-to-line})}$$

$$f_{con} = 20\,kHz \text{ (carrier frequency)}$$

Table 4.1 NPC–3 converter parameters

Assuming a nominal pulsated current amplitude value for the IGBT's of 25 A, the nominal power of the converter was calculated to be 7 kW. Inductances were chosen following [12] to limit the maximum current ripple to be less than 2% of the amplitude of the phase with the following formula:

$$L = \frac{V_{rms}/\sqrt{3}}{2\sqrt{6}\,f_{con}\,i_{ripple,peak}}$$

In the same way, capacitances were chosen to limit the voltage ripple to 2% for a nominal power Q_T, as follows:

$$C \geq \frac{Q_T}{6\,\omega\,Vc_d\,V_{ripple}}$$

Linearized transfer functions were obtained for each loop of the controller. For better performance, and in accordance with the time scale separation principle, bandwidth for the controller loops was chosen as depicted in **Table 4.2**:

LOOP	Transfer function	Intended bandwidth	Parameter estimates
tracking	$H_t(s) = \dfrac{1}{1 + \dfrac{L}{k_1}s}$	< 5837 rad/s	$k_1 \approx 17.5$
regulation	$H_r(s) = \dfrac{k_{i1} + k_{p1}\,s}{s^2 + k_{p1}\,s + k_{i1} + \dfrac{4\,s}{C\,R}}$	< 271 rad/s	$k_{p1} \approx 270$ $k_{i1} \approx 5500$
balance	$H_b(s) = \dfrac{k_{p2}}{\dfrac{2}{C\,R} + k_{p2} + s}$	< 13 rad/s	$k_{p2} \approx 4$

Table 4.2 Controller parameters estimated using the transfer function bandwidth. Notice that bandwidths are separated by 1.333 decades.

Starting from these estimates, manual tuning was performed to improve the overall response of the controller and schedule all control objectives as depicted in section 2.6. Finally, control parameter values were fixed to: $k_1 = 10$, $k_{p1} = 136$, $k_{i1} = 4500$, $k_{p2} = 2$ and $\gamma_k = 10000$, $\forall k \in H$, where $H = \{1,3,\cdots,21\}$. The desired voltage value Vc_d for each capacitor was set to $200V$. Notice that all involved parameters meet condition (3.29). Evaluation of expression (3.30), with V as defined in (3.26) and the aforementioned parameters, yields the following Lyapunov surface:

$$\frac{49\,511}{15\,264\,000}z_4^2 + \frac{11}{244}z_5^2 + \frac{1}{4\,500}z_4\,z_6 + \frac{613\,417\,729}{41\,976\,000}z_6^2 = 4.84 \times 10^6 \tag{4.1}$$
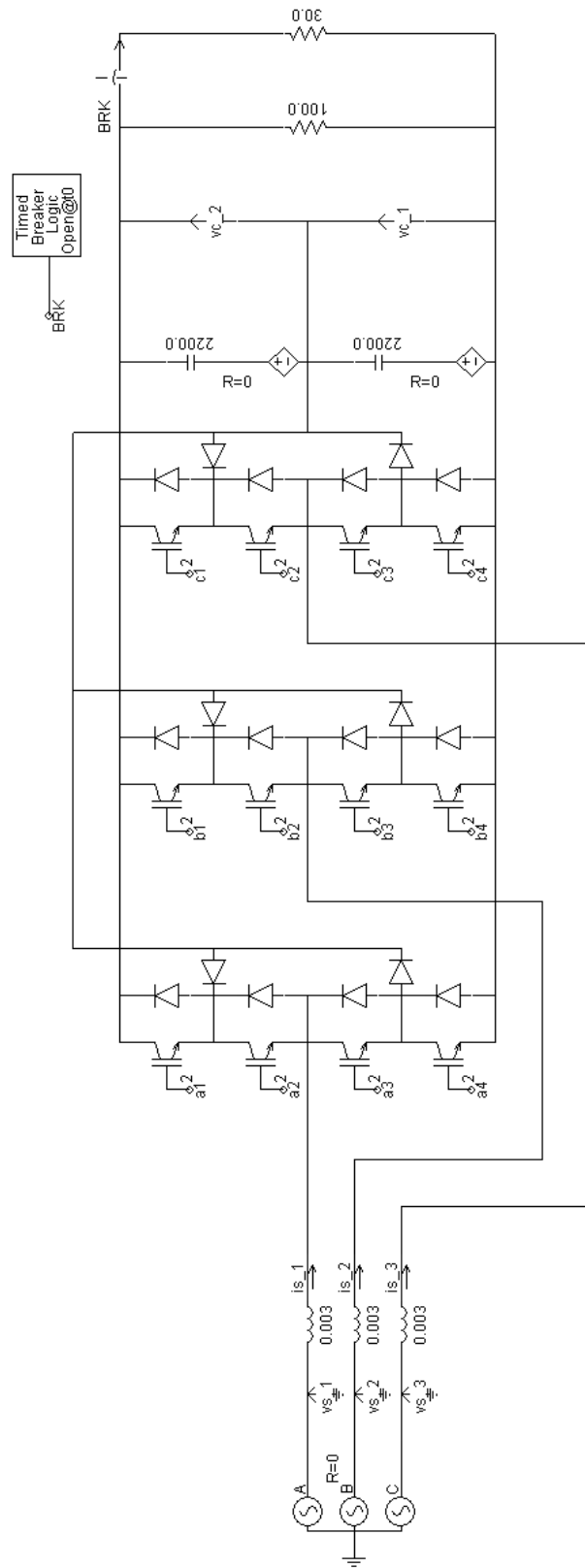
Figure 4.1 Snapshot of the PSCAD model

4.1 Start up response for initial conditions

Start up response for the system was evaluated using a resistive load of 100Ω.

Recalling from the definition $z_6 \triangleq x_6 + \dfrac{4Vc_d^{\;2}}{RCk_{i1}}$ in section 3.7, and setting the initial

value of the integrator x_6 to zero, it is straightforward to see that equation (4.1) can

be expressed in the original coordinates as:

$$1.13\times10^{-2}\left(Vc_1\left|Vc_1\right|-Vc_2\left|Vc_2\right|\right)^2+1.80\times10^{-2}\left(Vc_1\left|Vc_1\right|+Vc_2\left|Vc_2\right|-8\times10^4\right)+$$
$$8.11\times10^{-4}\left(Vc_1\left|Vc_1\right|+Vc_2\left|Vc_2\right|-8\times10^4\right)^2=4.46\times10^6$$

(4.2)

Now, equation (4.2) can be used to calculate a conservative estimate of a subset
of the region of attraction [22] in the original coordinates, when initial conditions are
zero for the integrator. This region is shown in Figure 4.2.
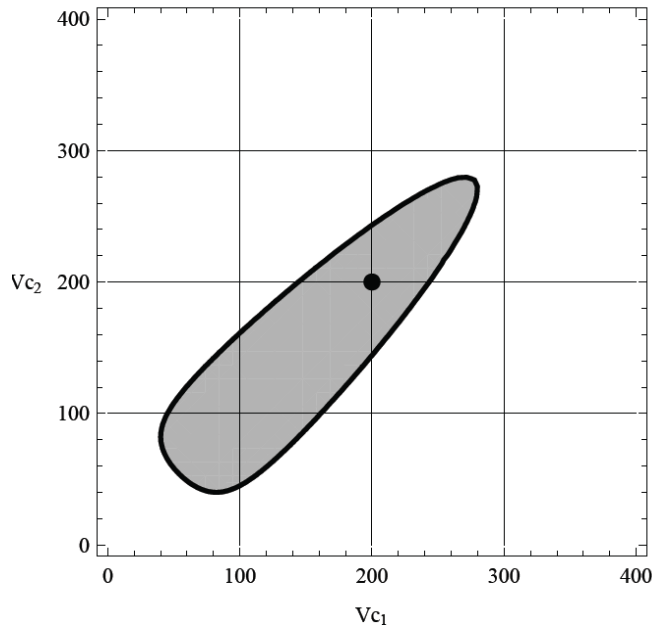
Figure 4.2 (gray) Estimate of a subset of the region of attraction
expressed in the original coordinates. The desired equilibrium point
is indicated with the black dot inside.

Hence, initial values for the capacitors' voltages can be chosen anywhere inside
the gray region. From Figure 4.2, it is important to point out that the origin of the

original coordinates ($Vc_1 = 0$, $Vc_2 = 0$) does not belong to the estimate of such a subset of the region of attraction. In fact, a preload process is carried out before the controller is set to work.

Remark 4.1 Observe from equation (2.21) that a given minimum voltage in the capacitors is necessary so that control inputs u_i, $i \in \{1,2,3\}$ do not saturate as $-1 \leq u_i \leq 1$, $i \in \{1,2,3\}$. This imposes a restriction on the equilibrium points allowed. Observe from equation (3.6) that the control input v_i, $i \in \{\alpha, \beta\}$ must be able to compensate for the voltage source term. Therefore, capacitors' desired voltage must be higher than the line's voltage.

To make the simulation more challenging, initial conditions were chosen at a point near the boundary of the Lyapunov surface and away from the line $Vc_1 = Vc_2$ to emphasize the fact that, unlike other approaches as [17], the model and controller proposed in this work do not assume initial balance of the capacitors. Therefore, initial values were set to $Vc_1 = 150\,V$ and $Vc_2 = 190\,V$. Figure 4.3 shows the capacitors' voltage response to the proposed initial conditions.
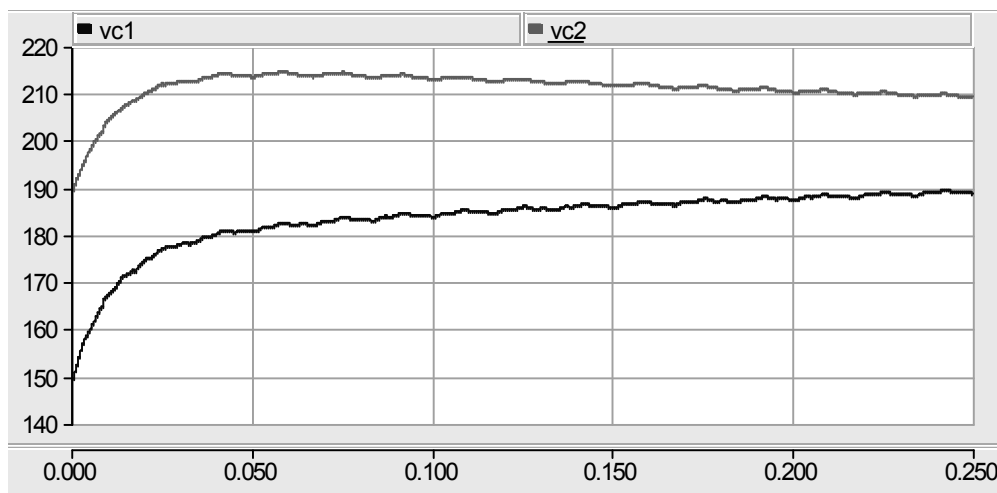
Figure 4.3 Transient response of capacitors' voltages to initial conditions.

The expression for the current reference signal (3.15) can be rewritten in the original *123*-coordinates as follows:

$$x_{123}^{*} = \left(g_1 + g_2 \frac{\sqrt{3}\, v_{s1}}{V_{rms}^2} \begin{pmatrix} 0 & 0 & 0 \\ 0 & -1 & 1 \\ 0 & 1 & -1 \end{pmatrix} \right) vs_{123}$$

Therefore, the transient disturbance is introduced in the phases 2 and 3 only. As a consequence, it is expected that phases 2 and 3 will be more distorted compared to phase 1 as observed in Figure 4.4.

Figure 4.5 shows the transient response to initial conditions for the control inputs u_i, $i \in \{1,2,3\}$ and v_i, $i \in \{1,2,3\}$. Also, the measured voltage across the ideal switches referred to point "0" is shown in the lower three graphs of Figure 4.5. As the measured voltages in the lower three graphs are modulated signals, switching within the values Vc_2, 0 and $-Vc_1$ a relatively high frequency, then they appear as a black stain composed of alternating squares. Notice that at the beginning the voltage level of such a square signal is lower than the expected value, and moreover, there is a clear unbalance between the positive and negative levels. This differences vanish as the time grows. Finally, notice that the white stripes in the measured voltages during the first cycle are due to transient saturation, which has not been considered in the present study.
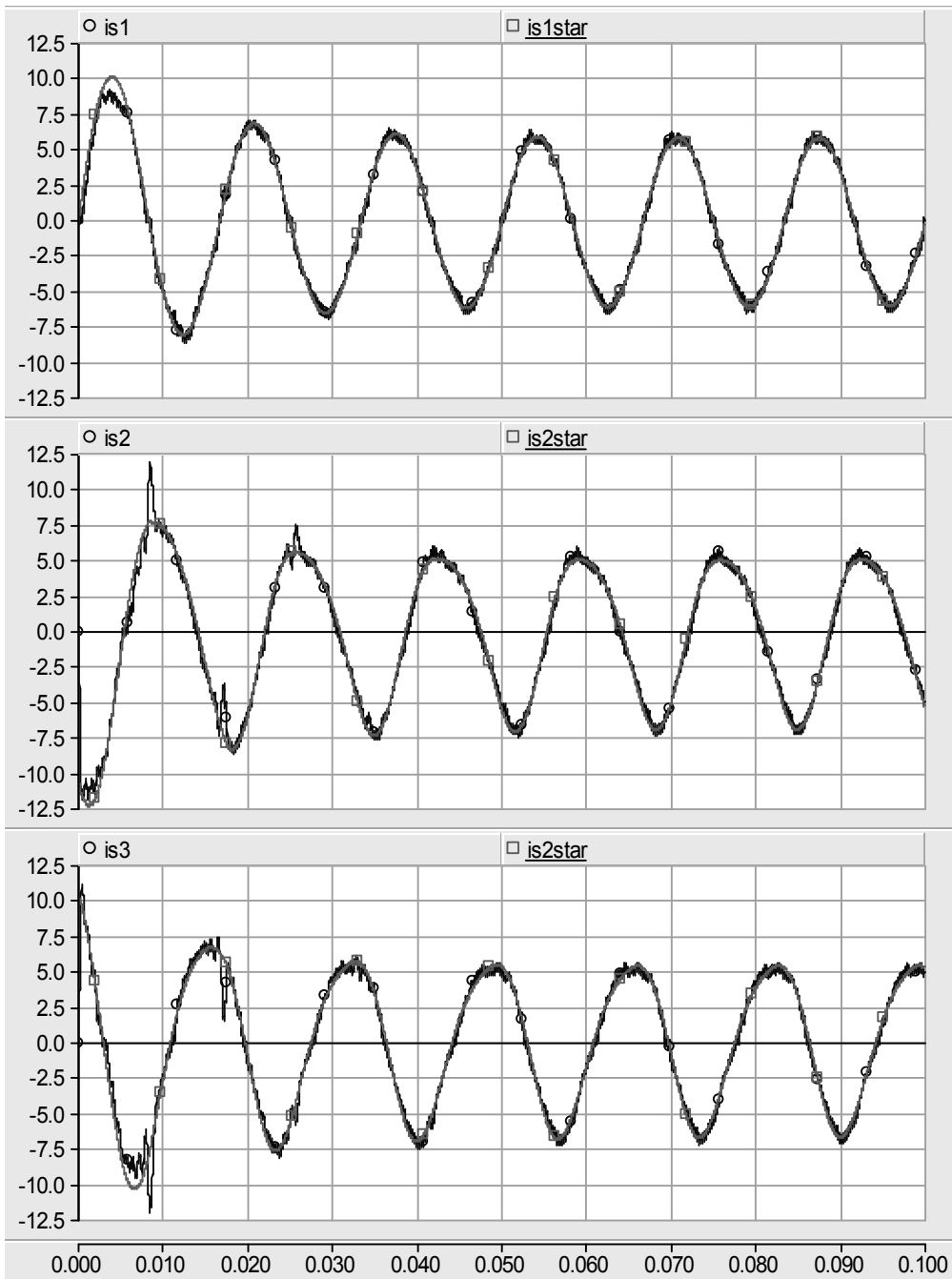
Figure 4.4 Transient response to initial conditions of inductors' currents along with their reference signals.
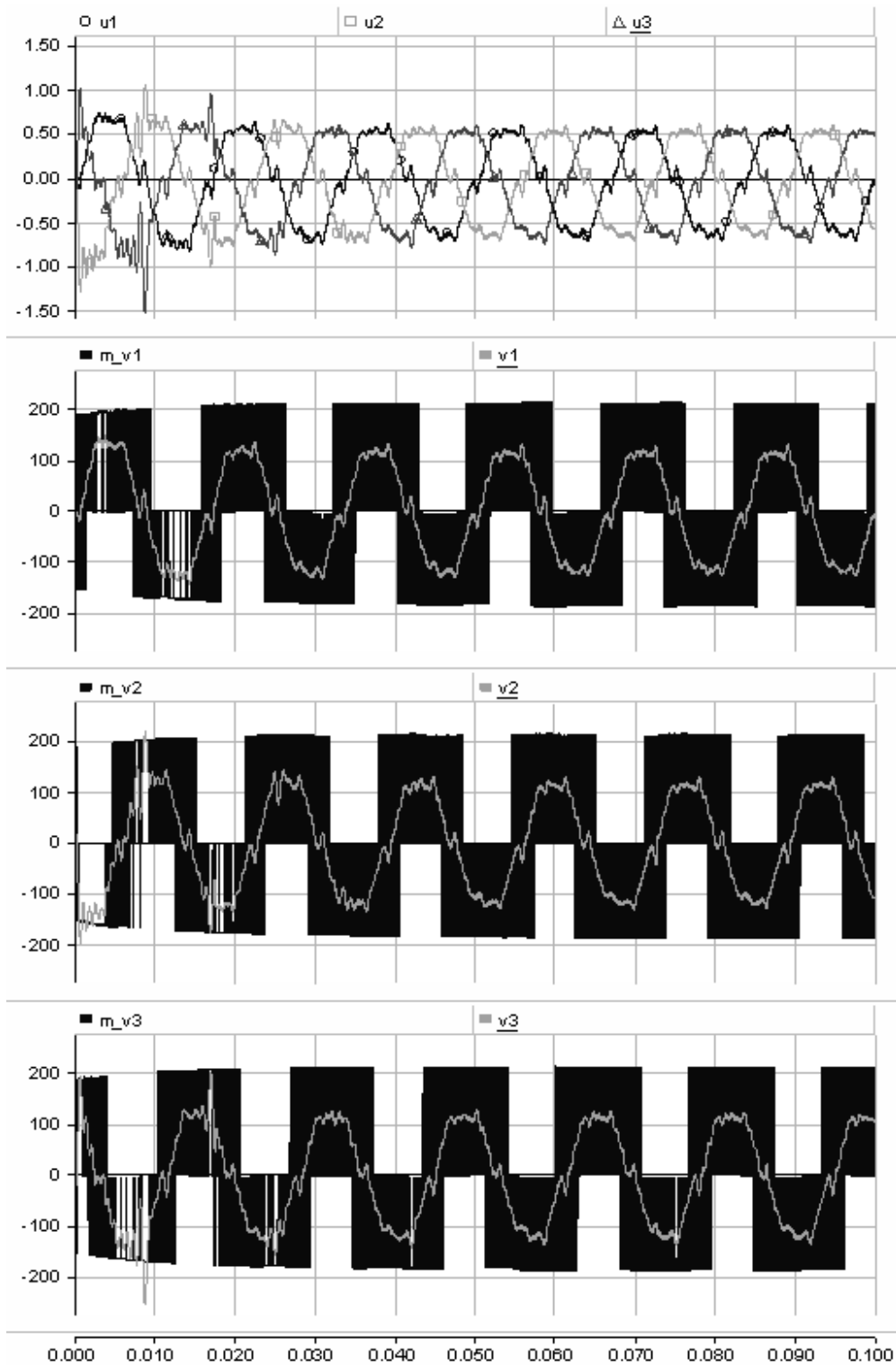
Figure 4.5 Transient response of all control inputs to initial conditions: (upper graph) original control inputs u_i, $i \in \{1,2,3\}$; (lower 3 graphs in gray) control inputs v_i, $i \in \{1,2,3\}$, (lower three graphs in black) the corresponding measured voltages.

Figure 4.4 shows that the tracking objective for the inductor's currents is achieved by time 0.025s. Figure 4.6 shows the state variables x_4 and x_5. Here notice that regulation is achieved by time 0.15 s and although complete balance is not accomplished, a steady state error is reached by time 2.5 s. Notice that all results are in accordance with the time scale separation principle.
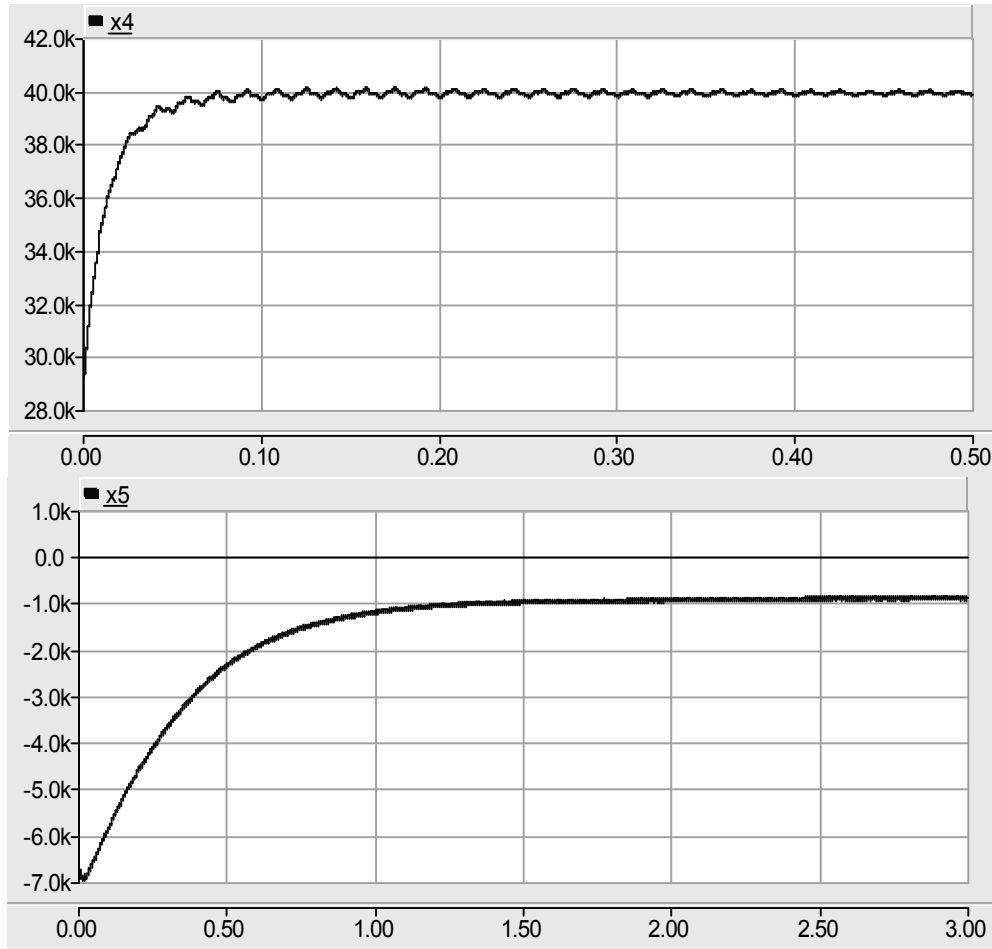
Figure 4.6 state variables x4 and x5 as defined in Chapter 4.

4.2 Steady state

Steady state response of the system was evaluated using a resistive load of 23Ω. The steady state behavior of the capacitors' voltages is shown in Figure 4.7. Note that the regulation objective is fulfilled, however, a relatively small steady state error prevents them to reach balance. However, a balancing capacity of 99% is

observed. Figure 4.8 shows the corresponding current steady state response. Notice the clean sinusoid shape of the currents, therefore illustrating a low THD.
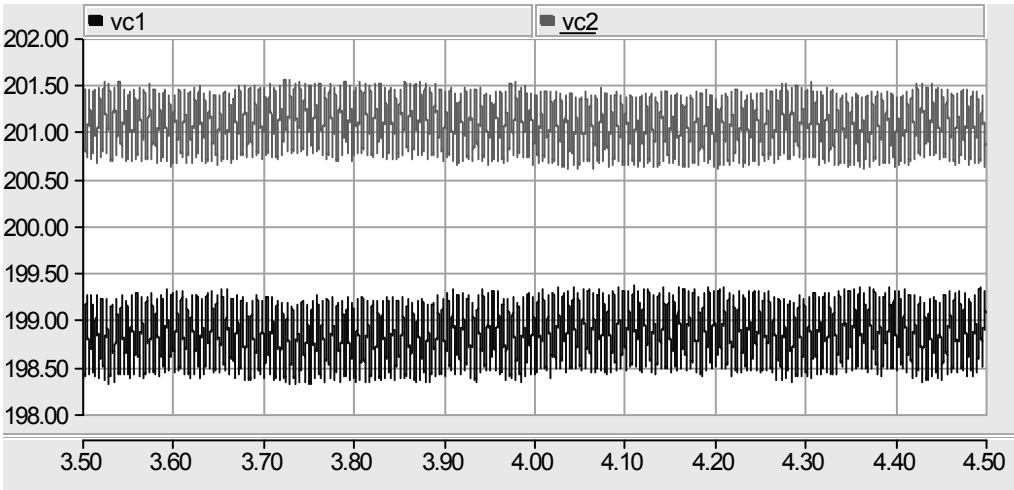

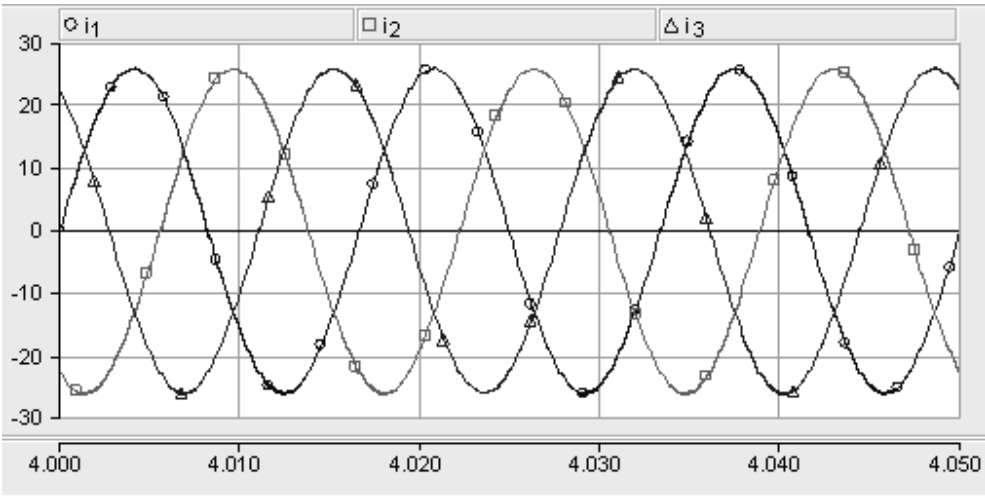**Figure 4.7** Steady state behavior of the capacitors' voltages

Figure 4.8 Steady state behavior of the inductors' currents

4.3 Load step change

The behavior of the system was investigated for a load step change from $100\,\Omega$ to $23\,\Omega$ at time $t = 3s$ and back to the original value of $100\,\Omega$ at time $t = 5.5\,s$. Figure 4.9 shows the capacitors' voltages transient response. Observe that the settling time of DC bus for this load change is about 0.3 s.

Figure 4.10 shows the corresponding transient response of the inductors' currents. Notice that both the inductor's current and the reference signal overlap, showing excellent tracking. A signal proportional to the source voltage is shown as well to point out that the current remains in phase with the voltage even during a load step change. The Total Harmonic Distortion (THD) of the inductor's currents was calculated during the step change showing average values of 3.5% and 1.2% for the $100\,\Omega$ and $23\,\Omega$ loads, respectively. Figure 4.11 shows the transient response for the THD of all three phases.
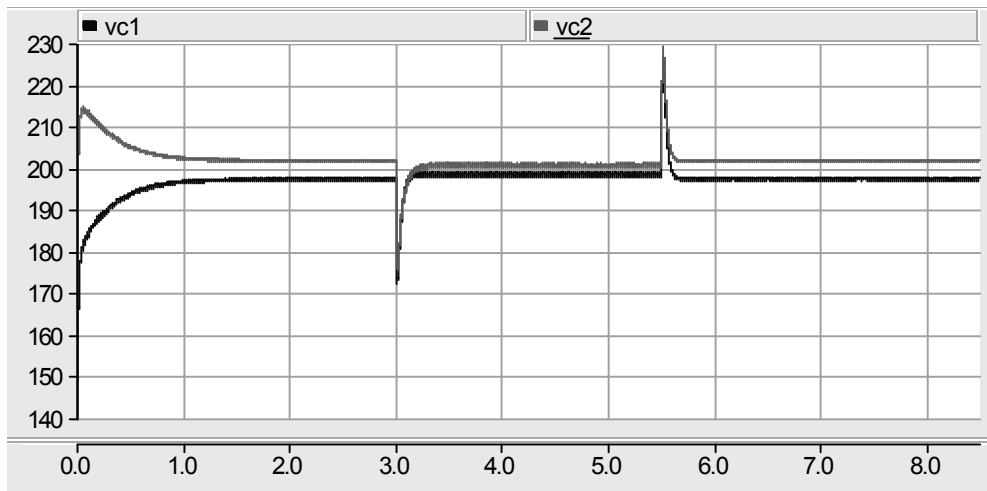

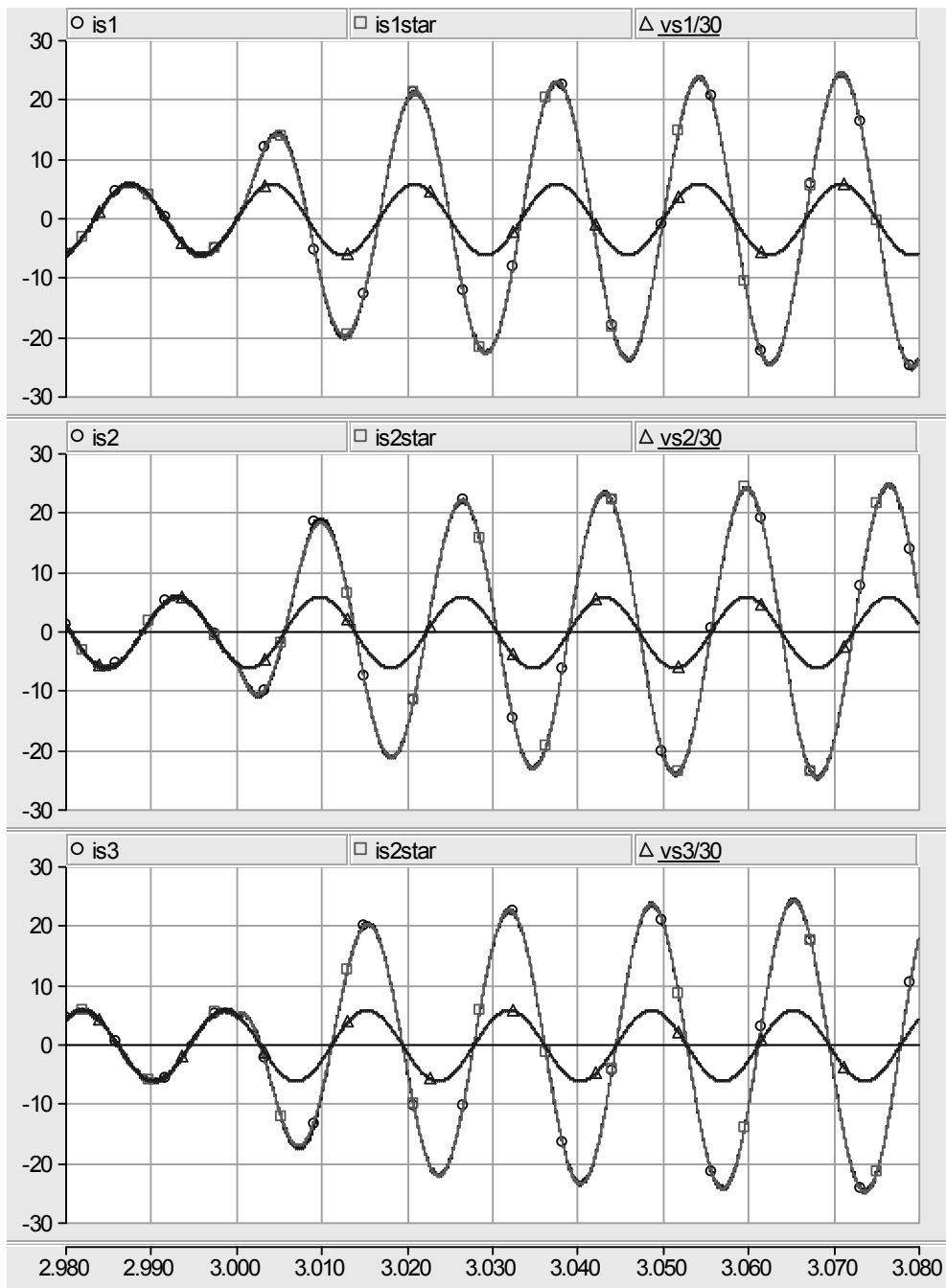**Figure 4.9** Transient response of the capacitors voltages during a load step change

Figure 4.10 Transient response of the inductor's currents to a load step change. (O) inductors' currents, (□) inductors' currents reference signals, and (△) the corresponding source voltages scaled by $1/30$.
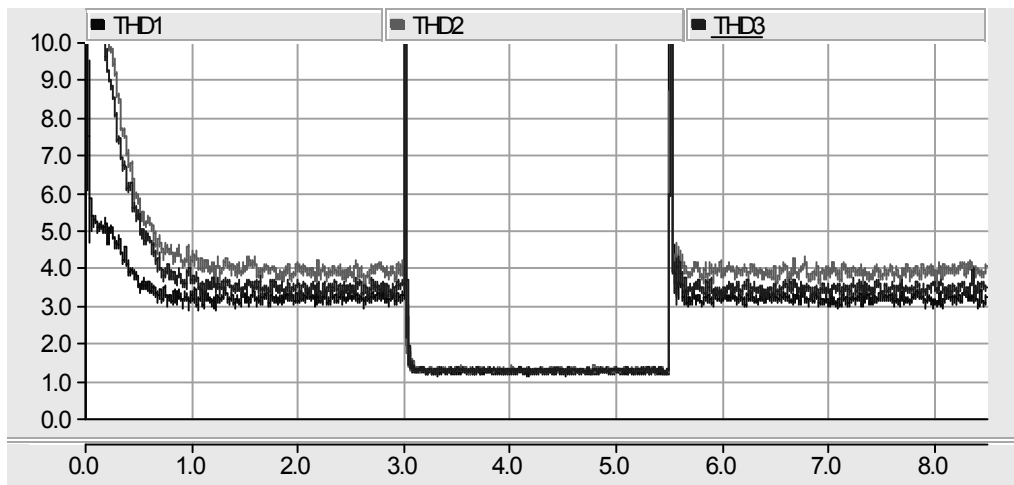
56

Figure 4.11 Transient response for the THD of the three inductors' currents.

4.4 Response to a voltage perturbation

To investigate the converter response to a voltage perturbation in one capacitor, a 20 V sudden drop is applied to capacitor 1, that is, an instant fall from 198 V to 178 V is introduced. Figure 4.12 shows the response of the capacitor's voltages to this perturbation. Notice that due to the *regulation* loop, the voltage of the capacitor 2 rises to compensate the voltage drop in the DC link rapidly. A time response of less than 1s is observed for the balance.
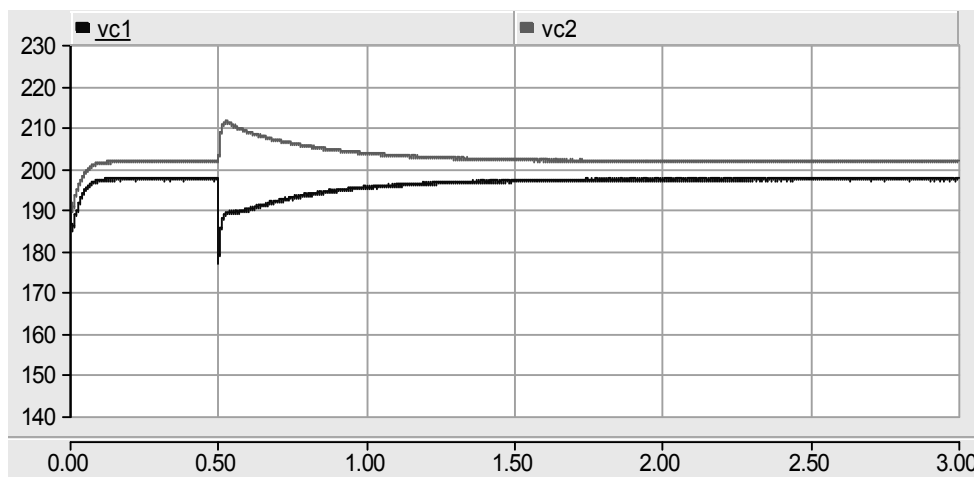

Figure 4.12 DC voltages transient response to a 20 V perturbation in capacitor 1.

Finally, Figure 4.13 shows the response of the inductors' currents to the aforementioned sudden voltage drop in capacitor 1. Notice that after a small transitory of about 0.025 s, currents recover their original sinusoid shape.
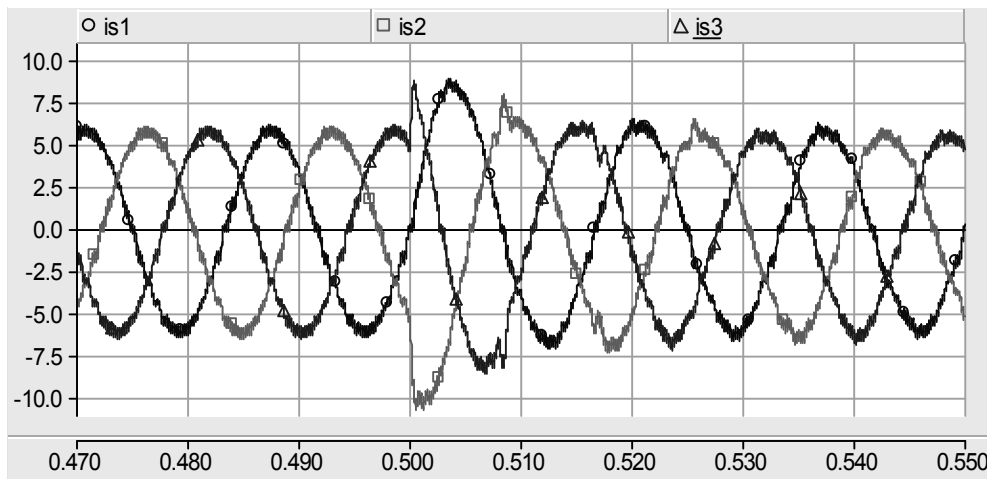

Figure 4.13 Currents transient response to a 20 V perturbation in capacitor 1.

4.5 Balance steady state error and THD tradeoff

Several numeric experiments were performed to try to reduce the steady state error in the balance of the capacitors' voltages. A straightforward approach suggests increasing the value of k_{p2}, however, this proved to interfere with the time scale separation principle leading to a poor overall behavior of the system. Hence, a different approach was investigated. Notice that the inner loop controller in equation (3.6) injects higher order harmonics to accomplish the tracking objective. This harmonic injection could add, in general, small DC contributions to the averaged model described in section 3.5, which were neglected to facilitate the design. For that reason, simulations were performed using a smaller bank of resonant filters considering $H = \{1,3,5,7\}$, that is, up to the 7-th harmonic. Figure 4.14 compares the steady state response of the capacitors' voltages along with the THD of their corresponding inductors' currents.
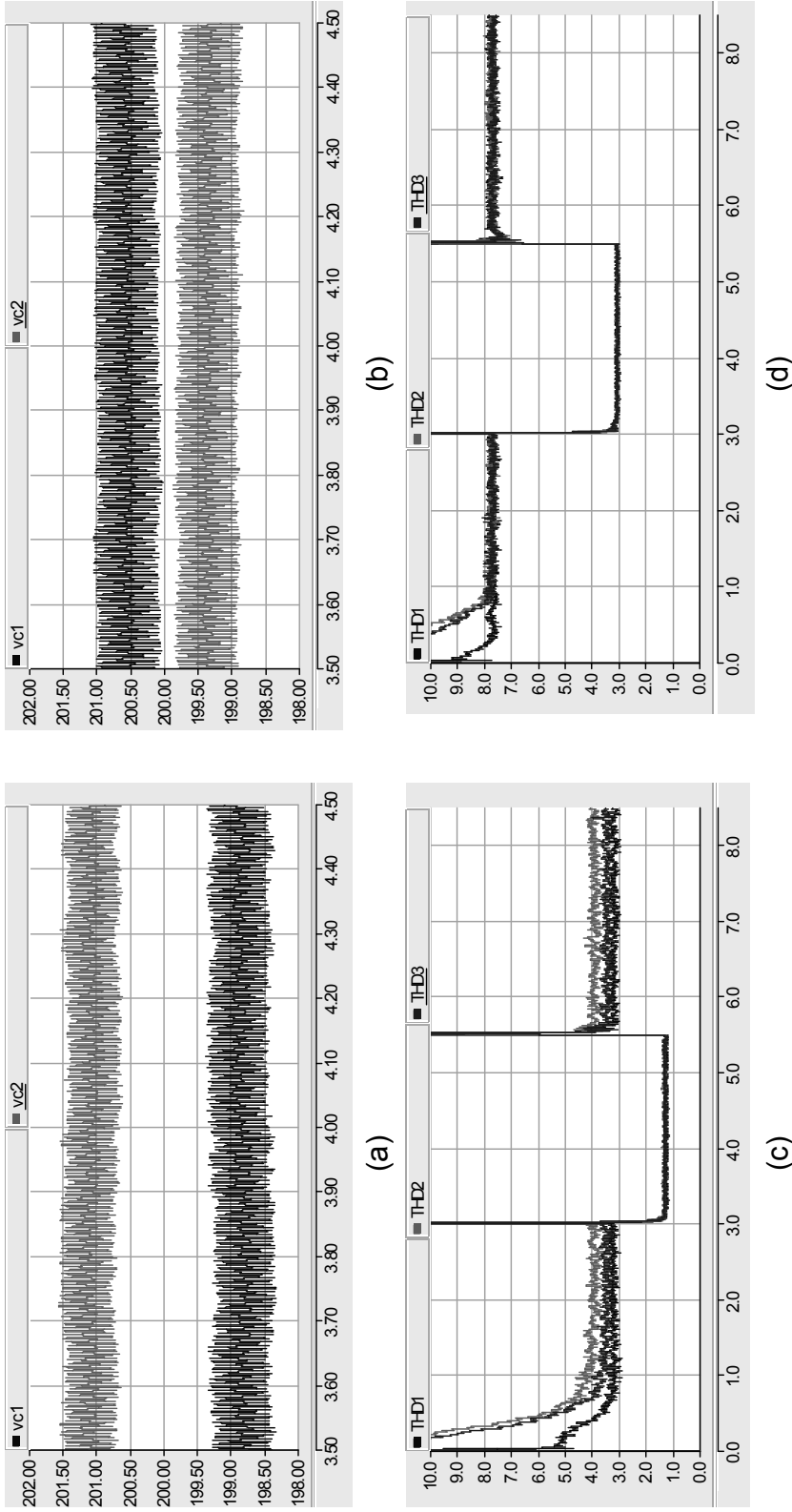
Figure 4.14 Steady state response of the capacitors' voltages using a bank of resonant filters compensating harmonics 1 to 21 (a) and 1 to 7 (b).The THD showed average values of 1.25% when harmonics 1 to 21 were compensated (c) and 3.1% when only harmonics 1 to 7 were taking into account (d). In both cases a 23 Ω load was used. Thus it is clear the tradeoff between THD reduction and capacitors' voltage balancing.

Chapter 5

Concluding remarks and future work

5.1 Conclusions

In this thesis work, the NPC–3 converter in a synchronous rectifier application was modeled via the Euler–Lagrange Formulation. It is Important to notice that the use of isomorphic transformations of both coordinate and control input allowed for a complete model suitable for control design purposes. Based on a time scale separation principle, control objectives –*tracking, regulation and balance*– were scheduled to be reached accordingly. For the control design purpose, a transitory perturbation was added to the current reference signal. Therefore, amplitude modulation of the unperturbed signal is used to accomplish the regulation objective, whereas the perturbation itself was employed as an extra control input to solve the balance objective. Based on the time scale separation principle, stability in the sense of Lyapunov was studied for the averaged capacitor's voltage dynamics.

To validate the proposed controller, simulations were performed using state of the art technical software. To emphasize the completeness of the proposed model, initial conditions for the capacitor's voltages were chosen close to the Lyapunov surface, away from the equilibrium point and the balanced state. Both tracking and regulation objectives were met as expected, however, a relatively small steady state error prevented from reaching total balance, in fact, an error of about 1% was observed between the two voltage levels. Further study of this balance issue

showed that the increasing number of resonant filters injecting harmonics to lower the THD of the inductors' currents was responsible for this behavior. Hence a tradeoff between THD reduction and capacitors' voltage balancing was observed. At this point, given that the main objectives required to provide with low THD (*tracking*) and a regulated DC link (*regulation*) are achieved, the small error in the *balance* can be neglected.

Finally, recall that although the time scale separation principle used, allowed for an easier controller design, bandwidth restrictions appeared, thus forcing the *regulation* and *balance* dynamics to have a slower response.

5.2 Future work

Other applications for the NPC–3 converter using the proposed controller such as shunt active filtering or back-to-back conversion are left for further research. As a constructive method for inserting transitory control inputs in the form of additional perturbing terms to the current reference signal was described, so, it is suggested that similar approaches could be used for other multilevel power converters, such as the NPC–5, three-level flying-capacitor or even the four-level flying-capacitor.

References

[1]   International Energy Outlook 2008 Energy Information Administration Office of Integrated Analysis and Forecasting U.S. Department of Energy Washington, DC 20585

[2]   IEEE Std. 519-1992: IEEE Recommended practices and requirements for harmonic control in electrical power systems. IEEE, 1992.

[3]   J.Lai, Peng F. "Multilevel converters- A new breed of power converters" IEEE Trans. Ind. Applicat., vol. 32, pp. 509–516, May/June. 1996.

[4]   Z. Pan, F. Z. Peng, V. Stefanovic, and M. Leuthen," A Diode-Clamped Multilevel Converter with Reduced Number of Clamping Diodes", in Applied Power Electronics Conf. (APEC´04), Anaheim, CA., Feb. 2004.

[5]   J.Rodriguez, J.Lai, Peng F. "Multilevel Inverters: A Survey of Topologies, Controls, and Applications" IEEE Trans. Ind. Applicat., vol. 49, pp. 724–738, Agost. 2002.

[6]   R. Teodorescu, F.Beaabjerg, J. K. Pedersen, E. Cengelci, S. Sulistijo, B. Woo, and P. Enjeti," Multilevel converters-A survey", in Proc. European Power Electronics Conf. (EPE ´99), Lausanne, Switzerland, 1999, CD-ROM.

[7]   A. Nabae, I. Takahashi, and H. Akagi, "A new neutral-point clamped PWM inverter", IEEE Trans. Ind. Applicat., vol. IA-17, pp. 518-523, Sept./Oct. 1981.

[8]   Brückner T., Bernet S., Güldner H. The Active NPC Converter and Its Loss-Balancing Control

[9]   IEEE PES Working group, FACTS applications, IEEE press, Publ. 96-TP-116, 1996.

[10]   H.Akagi and A. Nabae. "Control strategy of active power filters using multiple voltage source PWM converters" IEEE Trans. Ind. Applicat., vol. IA-22, pp. 460–465, May/June 1986.

[11]   Escobar, G. Leyva-Ramos, J. Carrasco, J.M. Galvan, E. Portillo, R.C. Prats, M.M. Franqueto, L.G. "Control of a three level converter used as a synchronous rectifier" Power Electronics Specialists Conference, 2004. PESC 04. 2004 IEEE 35th Annual

[12]   Fazel, S.; Bernet, S.; Krug, D.; Jalili, K.: Design and Comparison of 4-kV Neutral-Point-Clamped, Flying-Capacitor, and Series-Connected H-Bridge Multilevel Converters, IEEE Transactions on Industry Applications, Vol. 43, Nr. 4, August 2007, S. 1032-1040

[13]   Ralph Teichmann, Mariusz Malinowski and Steffen Bernet. Evaluation of Three-Level Rectifiers for Low-Voltage Utility Applications. IEEE TRANSACTIONS ON INDUSTRIAL ELECTRONICS, VOL. 52, NO. 2, APRIL 2005

[14]   Bin Wu, High-Power Converters and AC Drives. Wiley-IEEE Press, 2006. ISBN-13: 978-0471731719

[15]   J.M.A. Scherpen, D. Jeltsema and J.B. Klaassens, "Lagrangian Modeling of Switching Electrical Networks", Systems and Control Letters, Vol. 48, No. 5, 2003, pp. 365-374.

[16]   Herbert Goldstein, Charles P. Poole, John L. Safko. Classical Mechanics, Addison Wesley; 3rd Edition 2001. ISBN-13: 978-0201657029

[17]   Escobar, G. Leyva-Ramos, J. Carrasco, J.M. Galvan, E. Portillo, R.C. Prats, M.M. Franquelo, L.G. Modeling of a three level converter used in a

synchronous rectifier application. Power Electronics Specialists Conference, 2004. PESC 04. 2004 IEEE 35th Annual

[18]   G. Escobar, A.M. Stankovi´c and P. Mattavelli. "An Adaptive Controller in Stationary Reference Frame for D-Statcom in Unbalanced Operation," IEEE Trans. Ind. Electronics, Vol. 51(2), pp. 401-409, April 2004.

[19]   Escobar, G.; Valdez, A.A.; Martinez-Montejano, M.F.; Rodriguez, V.;"A model based controller for cascade multilevel converter used as a shunt active filter" 2007 IEEE Industry Applications Society Annual Meeting. September 23-27, 2007.

[20]   R. Ortega, A. Loria, P. J. Nicklasson, and H. Sira-Ramirez. Passivity based control of Euler-Lagrange systems. Springer-Verlag, 1998.

[21]   B. Francis and W. Wonham. "The internal model principle for linear multivariable regulators," Applied Mathematics and Optimization, Vol. 2, pp. 170-194, 1975.

[22]   Khalil, H. K. Nonlinear systems. Prentice Hall; 3rd edition, 2002. ISBN 0-13-067389-7

[23]   Escobar, G. Leyva-Ramos, J. Carrasco, J.M. Galvan, E. Portillo, R.C. Prats, M.M. Franqueto, L.G. "Modeling of a Three Level Converter Used in a Synchronous Rectifier Application" Power Electronics Specialists Conference, 2004. PESC 04. 2004 IEEE 35th Annual